# Performance of Drained and Undrained Flexible Pavement Structures under Wet Conditions

## Accelerated Test Data

## Test Section 544–Undrained

**Prepared for:**

**California Department of Transportation**

**by:**

**Manuel O. Bejarano, John T. Harvey, Abdikarim Ali,**
**David Mahama, Dave Hung, and Pitipat Preedonant**

**May 2004**

**Pavement Research Center**
**Institute of Transportation Studies**
**University of California at Berkeley and University of California Davis**

**TABLE OF CONTENTS**

**LIST OF FIGURES**

**LIST OF TABLES**

## EXECUTIVE SUMMARY

This report is the second in a series which describes the results of accelerated pavement testing on full-scale pavements conducted at the University of California Berkeley Pavement Research Center, located at the Richmond Field Station (RFS) in Richmond, California. The report contains a summary of the results and associated analysis of a pavement section composed of three lifts of asphalt concrete, untreated aggregate base, and subbase layers on top of a prepared subgrade. The pavement section is termed an "undrained pavement" because it does not include an asphalt treated permeable base (ATPB) layer between the asphalt concrete and untreated aggregate base layers. The pavement structure was designated Section 544. The tests conducted on this test section were performed as part of the Goal 5 Accelerated Test Program for the evaluation of drained (containing an ATPB layer) and undrained pavement under conditions of water infiltration.

The main objectives of the test program are:

1. to develop data to quantitatively compare and evaluate the performance of drained and undrained asphalt concrete pavements under "wet" conditions. Wet conditions intend to simulate approximate surface water infiltration rates that would occur in a pavement with a badly cracked asphalt concrete layer along the north coast of California during a wet month.
2. to measure the effectiveness of the drained pavement versus the undrained pavement in mitigating the effects of surface water infiltration on a reduction in stiffness of the unbound layers
3. Additional objectives include:

· to quantify elastic moduli of the pavement layers;

· to quantify the stress dependence of the stiffness moduli of the pavement layers;

- to determine the mechanism of failure of the pavement structure under these conditions
- to evaluate the effectiveness of non-destructive and partially destructive methods for assessing pavement structural condition.

HVS testing started in March 2000 and was completed in June 2000 after the application of more than $1.1 \times 10^6$ load repetitions. At the end of the test, the pavement section had 16 mm of surface rutting and a surface cracking density of 8.1 $m/m^2$.

Chapter 2 describes the test program for Section 544. Design thicknesses for the pavement components were:

| | |
|---|---|
| asphalt rubber hot mix | 40 mm |
| dense graded asphalt concrete | 162 mm |
| aggregate base | 274 mm |
| aggregate subbase | 305 mm |

Actual as-built thicknesses for the test section were:

| | |
|---|---|
| asphalt rubber hot mix | 51 mm |
| dense graded asphalt concrete | 149 mm |
| aggregate base | 272 mm |
| aggregate subbase | 205–310 mm |

The test program was conducted in four stages as follows:

- Stage 1: establish the initial structural condition of the section under conditions of no water infiltration
- Stage 2: establish the initial structural condition of the section under conditions of water infiltration
- Stage 3: HVS trafficking of the section under conditions of water infiltration
- Stage 4: establish the structural conditions of the test section after completion of HVS trafficking.

Data collection for Stages 1, 2, and 4 included deflections obtained using the falling weight deflectometer (FWD) and moisture content measurements. Stage 4 included some destructive and partially destructive tests to verify results obtained during Stage 3.

During Stage 3, loading was applied by dual radial tires inflated to a pressure of 720 kPa and consisted of the following loading sequence:

176,000 repetitions at a 40 kN load
211,000 repetitions at an 80 kN load
718,000 repetitions at a 100 kN load

At the termination of loading, surface rutting and fatigue cracking were visible throughout the test section. Data obtained during this stage is also summarized in Section 1 of this report.

Measures of pavement responses were obtained with Multi-Depth Deflectometers (MDDs), the Road Surface Deflectometer (RSD), and the laser profilometer. Fatigue cracking was monitored using digital photography and a digital image analysis procedure. Thermocouples were used to measure air and pavement temperatures at various depths in the asphalt concrete. To maintain a constant temperature of approximately 20ºC, a temperature control cabinet was utilized. Chapter 3 summarizes the data obtained during the course of loading and associated analyses.

The rutting data obtained for Section 544 and for previously tested sections indicated the impact of moisture content on the rutting performance of the section. Increased rutting was confined to the upper portion of the aggregate base layer. The rutting performance comparison between drained and undrained sections depended primarily on the trafficking load. Under the 40- and 80-kN loads, the performance of the drained section is superior to that of the undrained section. However, under the 100-kN load, stripping of the ATPB due to severe shear stresses and

water pumping action produced an increase in surface rutting. The failure in the ATPB prevented this layer from performing its expected function of draining water out of the pavement, and instead caused a reduction in the strength and stiffness of the aggregate base. Because of this failure in the ATPB layer, the undrained section was rated as having a better performance over the drained section.

## 1.0 INTRODUCTION

This report presents the data for the accelerated pavement testing (APT) program conducted using the Heavy Vehicle Simulator (HVS) on Section 544. This section is part of the accelerated test program described in the test plan for CAL/APT Goal 5, "Performance of Drained and Undrained Flexible Pavement Structures under Wet Conditions."(*1*)

Section 544 was tested to evaluate the performance of a typical California "undrained" pavement section under wet conditions and to compare its performance with that of Section 543 (a drained pavement section) in the same condition. From the Caltrans standpoint, an "undrained" pavement section is a conventional flexible pavement that does not have a permeable layer between the asphalt concrete and the aggregate base. A "drained" pavement section is a conventional flexible pavement that includes a 75-mm layer of asphalt treated permeable base (ATPB) between the asphalt concrete and aggregate base connected to a drainage system at the shoulder. The purpose of the ATPB layer is to intercept water entering the pavement, either through cracks in the asphalt concrete or through high permeability asphalt concrete, and carry it out of the pavement before it reaches the unbound materials layers where it may lead to a reduction in stiffness and resistance to rutting.

Wet conditions for Section 544 were intended to simulate surface infiltration rates that would occur along the north coast climate region of California during a wet month for a badly cracked asphalt concrete layer.(*2*) Because the pavement surface course of Section 544 was initially uncracked, water was introduced through small holes drilled through the asphalt concrete into the aggregate base.

## 1.1 Objectives

The main objective of this test program has been to evaluate the effectiveness of "drained" pavements in mitigating increases in moisture contents of the unbound materials (base, subbase, and subgrade) produced by surface water infiltration which can lead to a decrease in stiffness and an increase in rutting propensity of these materials. This objective can be accomplished by comparing the performance of drained and undrained pavements under wet conditions. Other objectives included the following:

- Determine the failure mechanism of the pavement section;
- Quantify elastic moduli of the various pavement layers using deflections obtained from a slow moving wheel and from the falling weight deflectometer (FWD);
- Evaluate the effectiveness of non-destructive and partially destructive methods for assessing the pavement structural condition; these methods included:
    a. Ground Penetrating Radar (GPR) and nuclear hydroprobes to measure water content, and
    b. FWD to estimate moduli of the pavement layers.

This report, together with similar reports for each of the other two test sections (543 and 545), an earlier published laboratory report (*3*), special associated reports, together with a summary report complete the test plan objectives for the Goal 5 program.

The sequence of HVS testing of the three Goal 5 test sections was: 1) Section 543 (drained), 2) Section 544 (undrained), and 3) Section 545 (undrained).

## 1.2 Organization of Report

Chapter 2 contains a description of the test program for Section 544, including loading sequence, instrumentation, and the data collection schedule. Chapter 3 presents a summary

together with analyses of the data collected during the test. These analyses included determination of backcalculated moduli from deflection tests and assessment of their effectiveness in establishing structural condition. Chapter 4 presents mechanistic analyses of Section 544 to evaluate and compare its performance to that of a section with an ATPB layer and two additional alternative sections. Chapter 5 contains a summary of the results and conclusions.

## 2.0 TEST PROGRAM

This section describes the test section layout, environmental conditions encountered during the test, instrumentation used to collect data, and the test program.

### 2.1 Test Section Layout

Section 544 is 8 m long by 1 m wide, with 16 stations at 0.5-m intervals in the longitudinal direction, as shown in Figure 1. The pavement was constructed with a two-percent cross slope and a 0.5-percent longitudinal slope in all layers above the aggregate subbase. Design and as-built layer thicknesses for the pavement are summarized in Table 1. As-built pavement thicknesses were obtained from measurements in the non-trafficked areas of a trench excavated at the completion of HVS trafficking.

**Table 1 Pavement Layer Thicknesses for Section 544**

| Layer | Design (mm) | As-built (mm) |
|---|---|---|
| Asphalt Rubber Hot Mix-Gap Graded | 40 | 51 |
| Asphalt Concrete | 162 | 149 |
| Aggregate Base | 274 | 272 |
| Aggregate Subbase | 305 | 205-310 |

### 2.2 Environmental Conditions

The accelerated pavement test was conducted under wet conditions at moderate pavement temperatures. Wet conditions were simulated by introducing water into the aggregate layers by means of a drip infiltration system. The infiltration system consisted of a series of 2.5-cm holes drilled through the asphalt concrete at 0.5-m intervals along a 12-m length just outside the trafficked area of the pavement (Figure 1). Drip hoses were inserted in each hole and attached to a main pump and timing system. At the end of each drip hose was a nozzle which regulated the flow. Figure 2 is a photograph of the system in place.

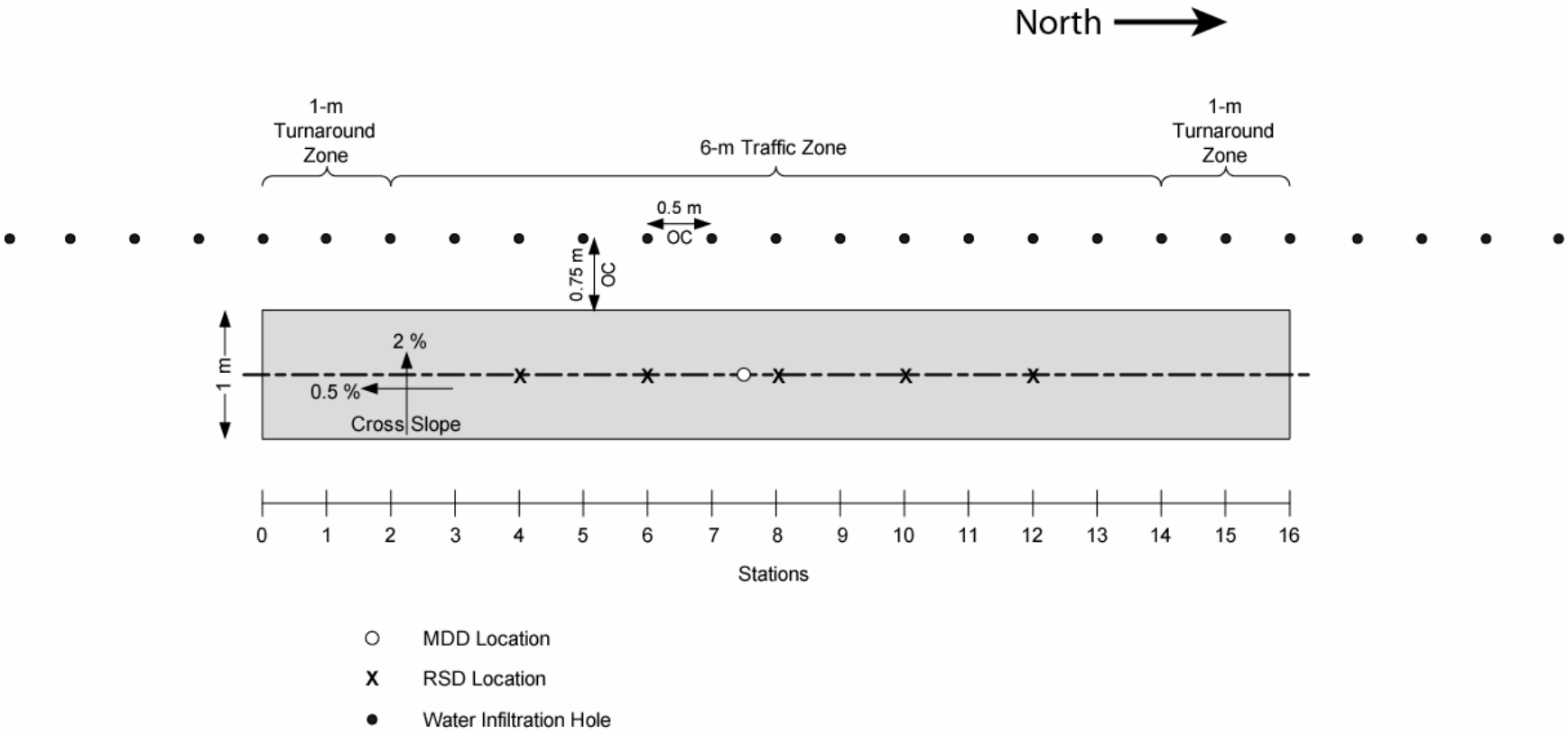


**Figure 1. Test section layout and instrumentation.**

**Figure 2a.**

**Figure 2b.**

**Figure 2. Water infiltration system on Section 544..**

The design rate of water infiltration into the aggregate base was 9.7 liters per hour over an area 7.4 m wide by 12 m long. This flow was calculated to simulate precipitation for an average peak week in Eureka of 51.3 mm rainfall.(*2*) However, because the rate at which the aggregate base would accept water infiltration was lower than the design rate, the flow was reduced to the maximum possible (approximately 0.4 liters per hour).

The target pavement temperature at a pavement depth of 50 mm of 20 ± 2°C was maintained by a temperature control box.

## 2.3 Instrumentation

Instrumentation installed on Section 544 included 1) Multi-Depth Deflectometers (MDD) to measure deflections and permanent deformations at various depths in the pavement section, 2) laser profilometer to monitor surface rutting, 3) Road Surface Deflectometer (RSD) to measure surface deflections, 4) thermocouples to monitor pavement temperatures, and 5) nuclear hydroprobes and tensiometers to monitor moisture content in the unbound layers. Figure 1 shows the section layout and location of RSD, MDD, and laser profilometer measurements; Figure 3 shows the vertical location of MDDs and thermocouples in Section 544. For a complete description of the instrumentation used for this study, refer to Reference (*3*).

## 2.4 Test Program

Evaluation of the performance of the test section included four stages as shown in Figure 4. These stages can be summarized as follows:

- Stage 1: Testing and evaluation of the pavement section prior to water infiltration. Water measurements and FWD testing were conducted to establish initial conditions and structural capacity.

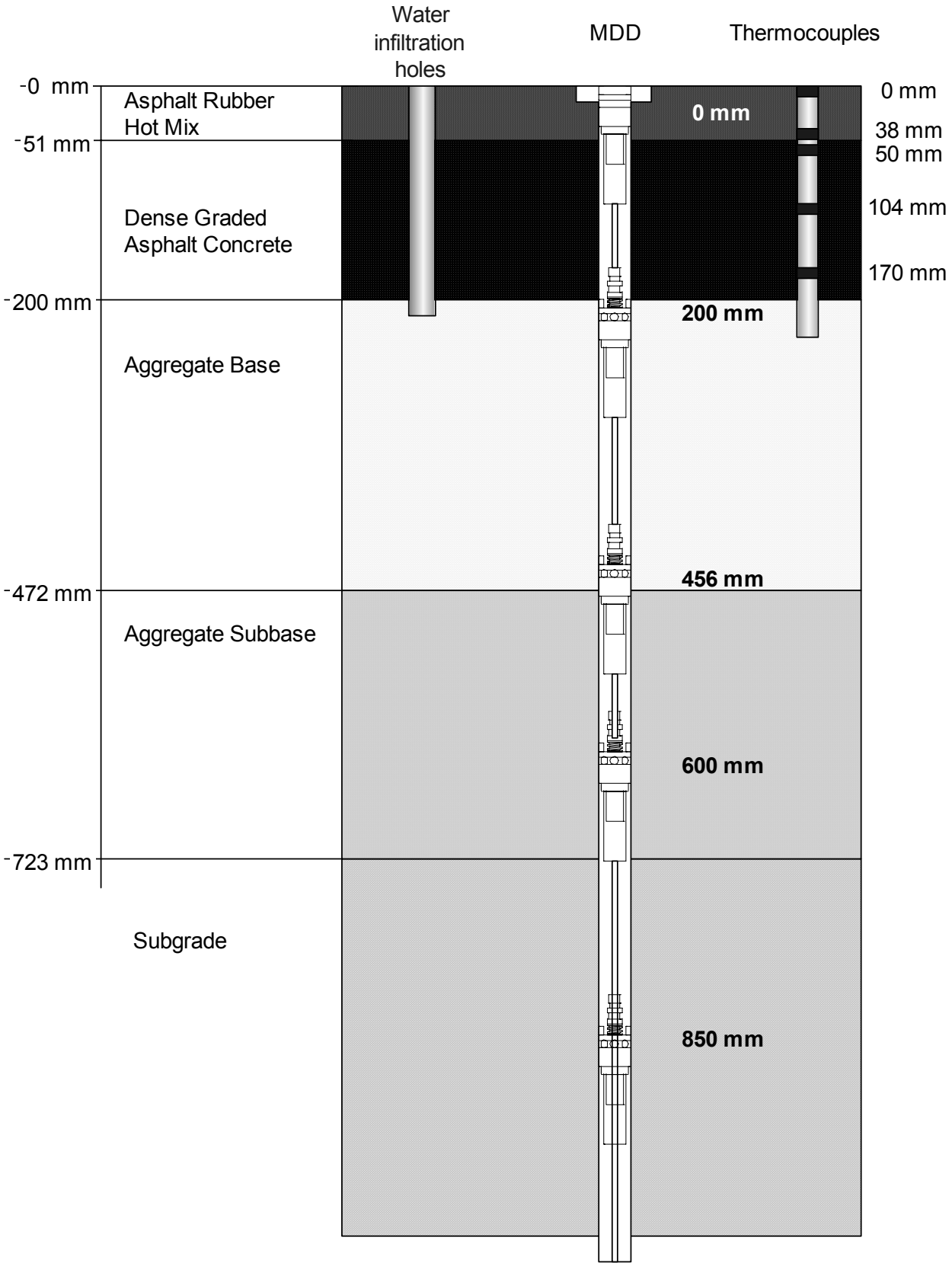


**Figure 3. Location of MDDs and thermocouples in Section 544.**

## Section 544 Test Program Schedule

| ID | Task Name |
|---|---|
| 1 | **Stage 1: Dry Base** |
| 2 | Section 544 |
| 3 | **Stage 2: Wet Base** |
| 4 | Section 544 |
| 5 | **Stage 3: HVS Testing on Wet Base** |
| 6 | Section 544 |
| 7 | HVS Upgrade |
| 8 | **Stage 4: Forensic Activities** |
| 9 | **Section 544** |
| 10 | Coring, DCP |
| 11 | Test Pit |

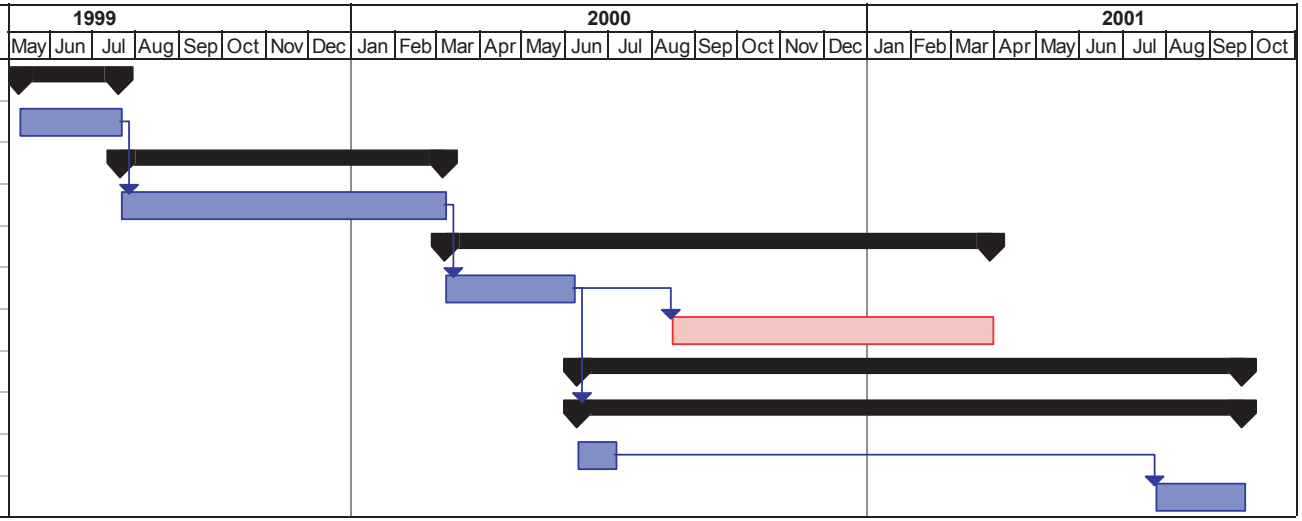


**Figure 4. Section 544 test program schedule.**

- Stage 2: Testing and evaluation of the pavement section during water infiltration. Water measurements and FWD testing were conducted to establish conditions and structural capacity prior to testing.
- Stage 3: HVS testing of the pavement section with water infiltrating the pavements. During loading, the pavement sections was monitored using the instrumentation noted in Section 2.3.
- Stage 4: Evaluation of the pavement section at the conclusion of HVS trafficking by means of FWD testing, trenching, and sampling of the pavement materials. Trenching and sampling of the materials were conducted simultaneously with forensic activities on Section 545.(*4*) Section 545 was tested after upgrades were made to the Heavy Vehicle Simulator.

### 2.4.1 Falling Weight Deflectometer (FWD) Testing

FWD testing was conducted from July 1999 to July 2001 to monitor surface deflections and changes in moduli of the pavement layers during all three stages of testing. Target testing loads of 20, 40, and 60 kN were used and the surface deflections normalized to a 40-kN load for analysis. Sensors were spaced at 0, 200, 300, 600, 900, 1200, and 1500 mm from the loading plate. Backcalculated moduli were obtained for the three load levels considered.

### 2.4.2 Heavy Vehicle Simulator Trafficking

For trafficking of Section 544, the HVS was equipped with dual truck tires, representing one half of a single axle. Load was applied through two Goodyear radial tires (G159 11R 22.5) inflated to a pressure of 720 kPa. Three load levels were used. Table 2 summarizes the loading sequence.

**Table 2 Applied Trafficking Loads in Section 544**

| Trafficking Load (kN) | HVS Repetitions |
|---|---|
| 40 | 0 to 176,290 |
| 80 | 176,290 to 387,027 |
| 100 | 387,027 to 1,105,123 |

The test wheel trafficked the entire length of the 8-m test section. Lateral wander over the 1-m width of the test section was programmed to simulate traffic wander on a typical highway lane. Pavement performance was evaluated for the 6 × 1 m area between reference points 2 and 14 in which the HVS wheel speed is constant; the 1-$m^2$ areas at both ends of the trafficked area (Stations 0–2 and 14–16) serve as "turnaround zones" in which the test wheel decelerates and accelerates (Figure 1).

### 2.4.3 Data Collection

Table 3 summarizes the data collection sequence for Section 544.

**Table 3 Data Collection Program**

| Load Applications | Laser Profilometer | Multi-Depth Deflectometer | Road Surface Deflectometer | Crack Monitoring |
|---|---|---|---|---|
| 0 | X | 40 kN | 40 kN | |
| 15632 | X | 40 kN | 40 kN | |
| 50955 | X | 40 kN | 40 kN | |
| 90255 | X | 40 kN | 40 kN | |
| 116286 | X | 40 kN | 40 kN | |
| 147583 | X | 40 kN | 40 kN | |
| 176290 | X | 40 kN | 40 kN | |
| 203917 | X | 80 kN | 80 kN | |
| 227947 | X | 40 kN | 40 kN | |
| 279942 | X | | | |
| 243305 | X | 40, 80 kN | 40, 80 kN | |
| 312525 | X | 40 kN | 40 kN | |
| 341600 | X | | | |
| 358420 | X | 40 kN | 40 kN | |
| 387027 | X | 40, 60, 80, 100 kN | 40, 60, 80, 100 kN | |
| 427663 | X | 40, 100 kN | 40, 100 kN | |
| 467543 | X | 40, 100 kN | 40, 100 kN | X |
| 495141 | X | 40, 80, 100 kN | 40, 80, 100 kN | |
| 525914 | X | 40, 60 kN | 40, 100 kN | |
| 541103 | | 40, 100 kN | 40, 60 kN | X |
| 582476 | X | 40, 100 kN | 40, 100 kN | |
| 683008 | X | 40, 100 kN | 40, 100 kN | |
| 667477 | | | | X |
| 761737 | X | 40, 100 kN | 40, 100 kN | |
| 841314 | X | 40, 100 kN | 40, 100 kN | |
| 916064 | X | 40, 100 kN | 40, 100 kN | |
| 952195 | | | | X |
| 954507 | X | 40, 100 kN | 40, 100 kN | |
| 1105123 | X | 40, 100 kN | 40, 100 kN | X |

## 3.0 SUMMARY OF TEST DATA

This chapter provides a summary of data collected during the four stages of testing and include temperature and moisture conditions, permanent deformation, elastic deflection, crack progression, FWD deflection, and post-HVS test forensic and destructive test data.

### 3.1 Temperature, Rainfall, and Moisture Content Data

Temperature and moisture content data were obtained throughout testing of Section 544. The following sections summarize these data.

#### 3.1.1 Temperature Data

Figure 5 shows average daily air temperatures inside Building 280 at the RFS in which the HVS tests were conducted together with average air temperatures inside the HVS temperature control box. The average daily temperatures were calculated from hourly temperatures recorded during testing. Average air temperatures monitored in the temperature control box were uniform with minimal variations with an average air temperature value of 20.5°C. The average air temperature in the building was 17.9°C during the same period.

Average daily asphalt concrete temperatures for Section 544 are shown in Figure 6. These temperatures were recorded at various depths in the pavement including the ARHM top layer and both lifts of the asphalt concrete. The temperatures at depth were fairly uniform and varied slightly with air temperature above the test section. Average temperature in the asphalt concrete layers was 20.2ºC, approximately 1.5 percent less than the average air temperature.

#### 3.1.2 Rainfall and Moisture Content Data

Figure 7 shows average monthly rainfall data from the National Weather Service weather station in Richmond, CA during the four stages of testing of Section 544.

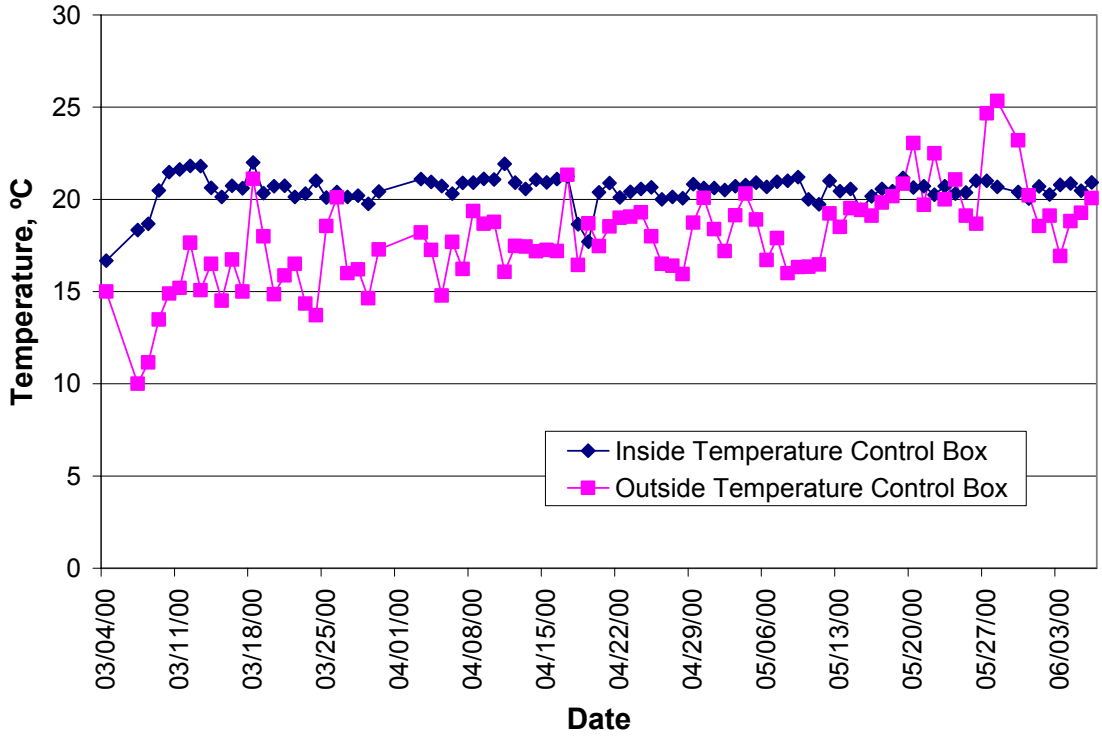


**Figure 5. Average air temperatures inside and outside HVS temperature control box, Section 544.**

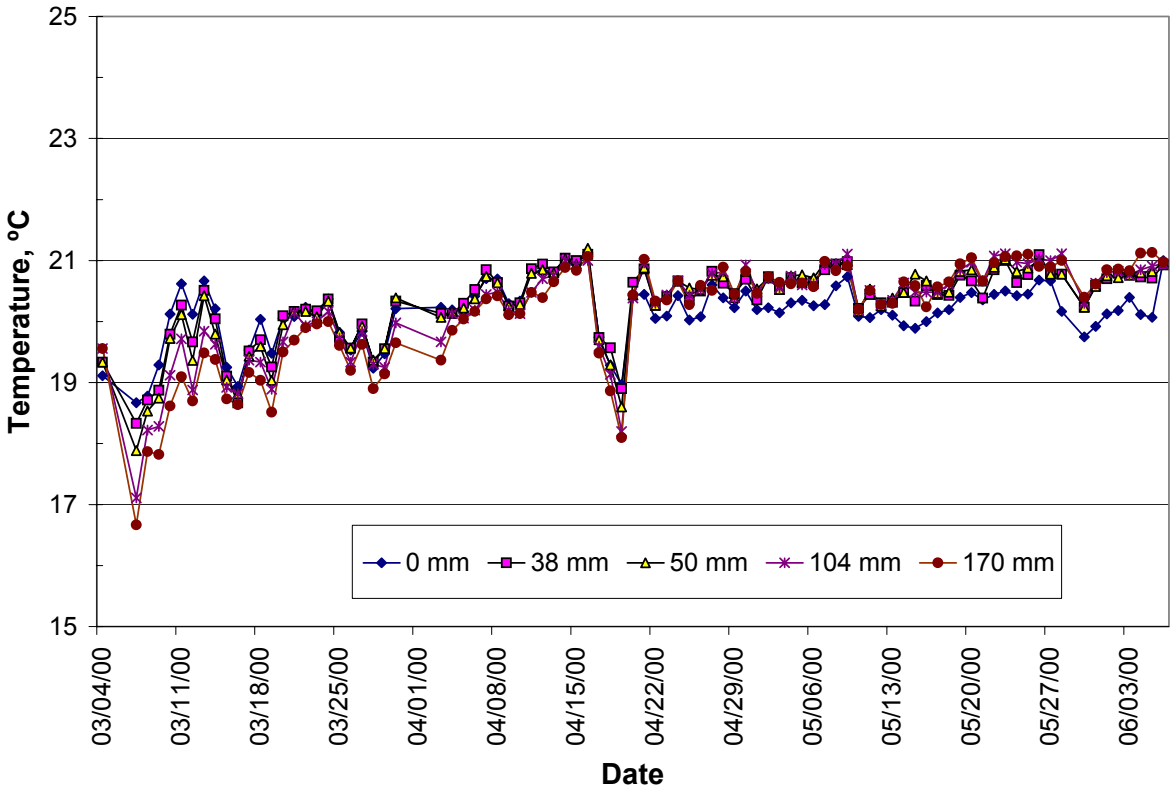


**Figure 6. Pavement temperatures at depth, Section 544.**

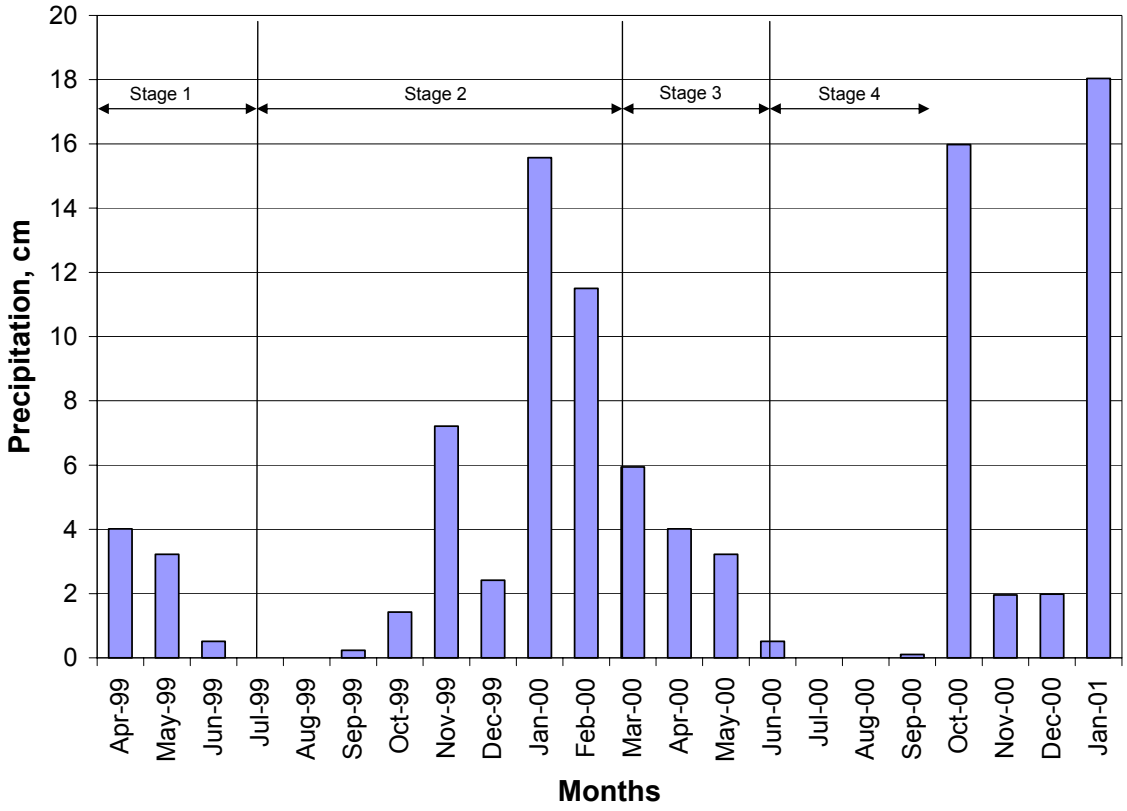


**Figure 7. Monthly precipitation for Richmond weather station during testing of Section 544.**

*3.1.2.1 Hydroprobe data*

Average volumetric moisture contents for the aggregate base, subbase, and subgrade materials obtained using a hydroprobe device are shown in Figures 8 and 9. Measurements for the aggregate base and subbase were obtained at depths of 320 and 586 mm from the pavement surface, respectively, while hydroprobe readings for the subgrade were obtained at pavement depths of 859, 1159, and 1735 mm.

Volumetric moisture contents of the base and subbase were averaged across measurements taken for those layers. Figure 8 shows that the moisture content of the untreated bases remained relatively constant through all stages of testing. Moisture contents were expected to increase at least in the aggregate base due to water infiltration.

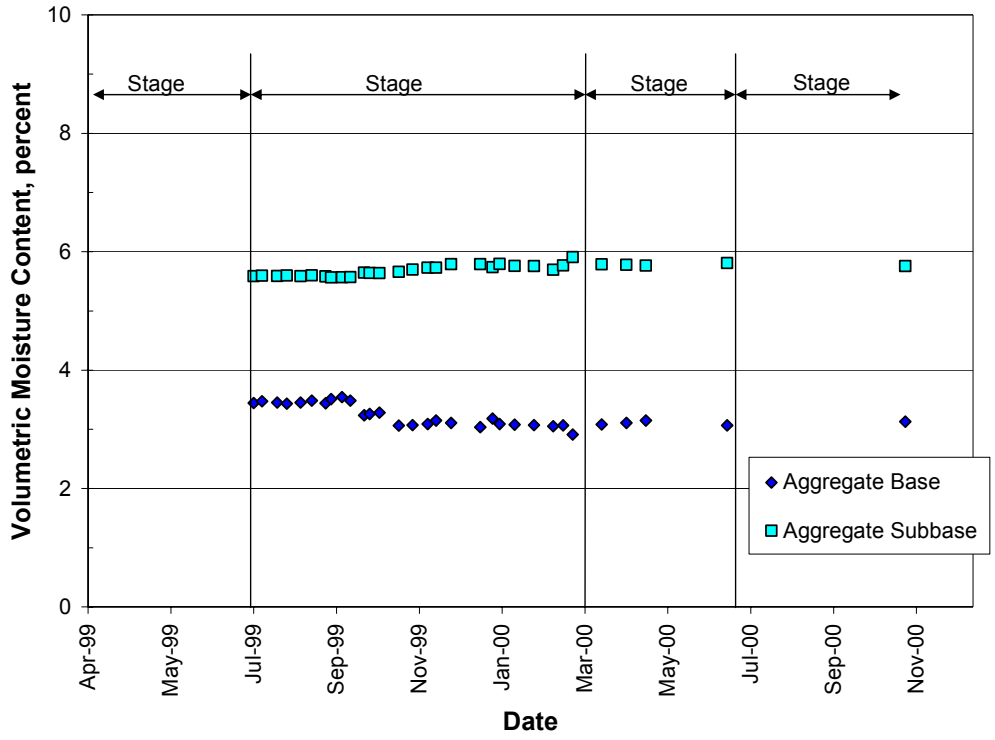


**Figure 8. Volumetric moisture content in the aggregate base and subbase.**

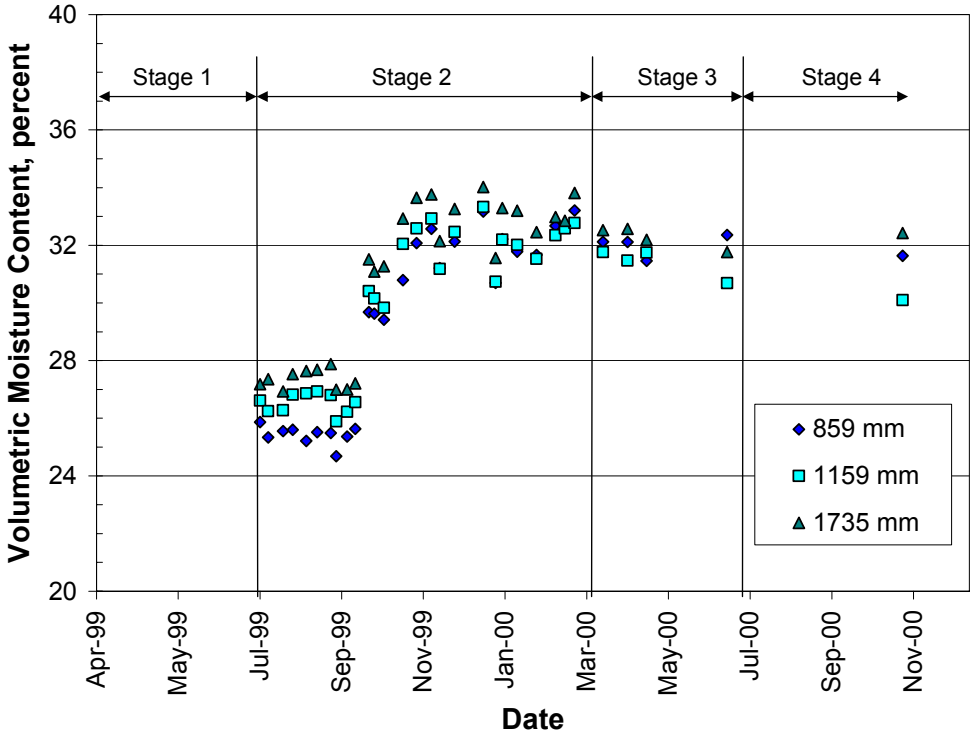


**Figure 9. Volumetric moisture content in the subgrade.**

Moisture contents for the subgrade (Figure 9) exhibit changes in line with precipitation trends (Figure 7). This was expected since the subgrade at the test site was not isolated from the surrounding soil; therefore it was subjected to the seasonal moisture variations at the site.

#### *3.1.2.2 Ground Penetrating Radar (GPR)*

Moisture contents in the aggregate base and aggregate subbase were also determined by GPR. While these data were collected periodically throughout the four stages of testing, only the results of Stage 4 are presented in this report. A comprehensive GPR report (*5*) is available as part of the Goal 5 program.

The radar equipment used in this study was a Sensors and Software Inc. PulseEkko 1000 surface GPR system. Details of the equipment, data processing, and moisture content estimation are given in Reference (*5*).

After HVS testing (Stage 3), a GPR survey was performed and the asphalt concrete was cored immediately afterwards at several locations to obtain gravimetric moisture contents in the untreated base materials (see Section 3.6 for a description of the coring activities). Gravimetric measurements were taken every 2-3 cm in the aggregate base and subbase layers, and were converted to volumetric moisture contents using the density of the layers. These measurements were then averaged across the thickness of each layer for comparison to the GPR-derived volumetric moisture content estimates from the final survey. Figure 10 shows the gravimetric moisture contents for the eight locations. Comparison of GPR and volumetric moisture contents estimated from gravimetric moisture contents for the aggregate base and subbase are shown in Figures 11 and 12, respectively.

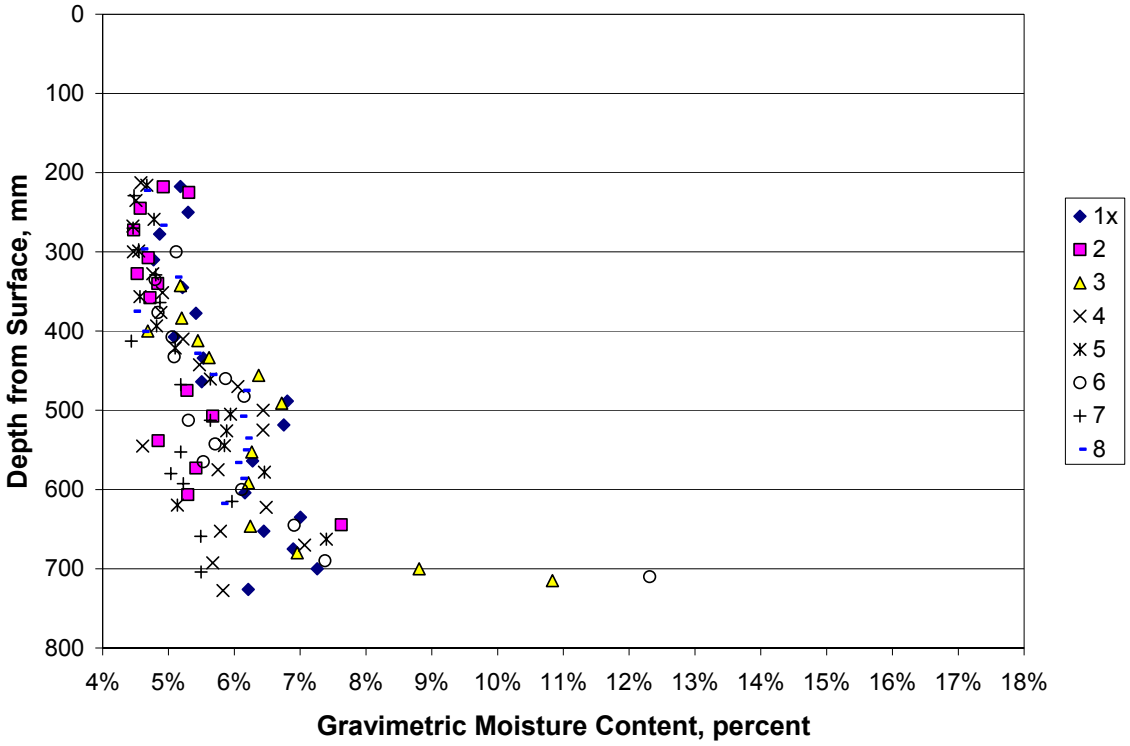


**Figure 10. GPR-derived gravimetric moisture contents for Section 544.**

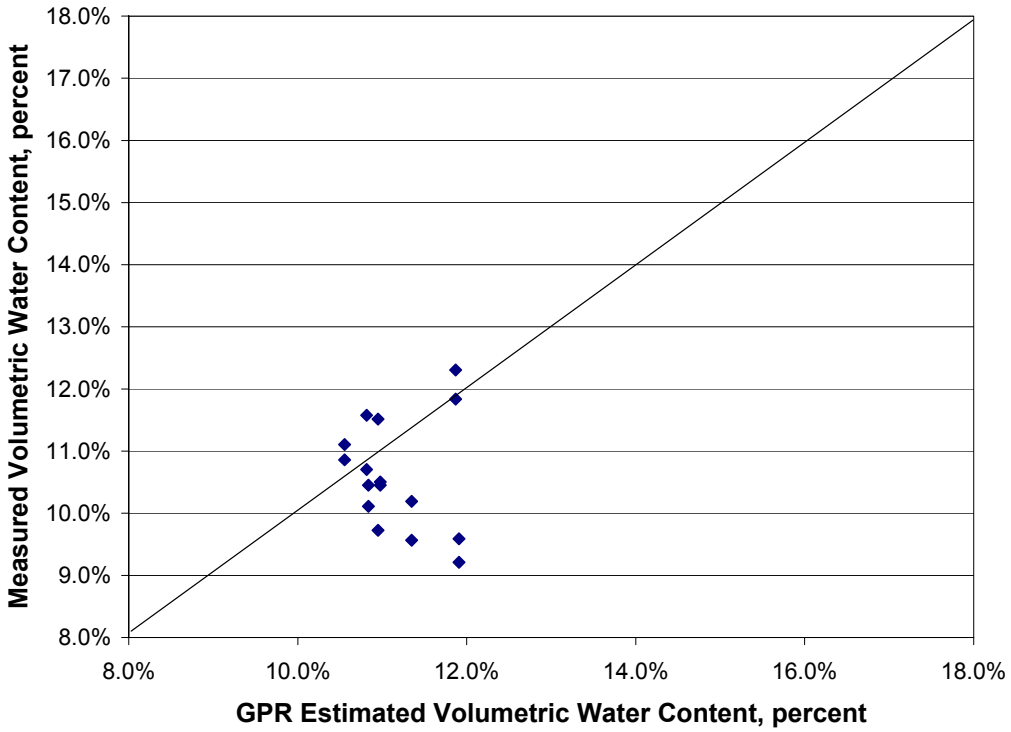


**Figure 11. Comparison of GPR and gravimetric estimated volumetric aggregate base moisture contents for Section 544.**

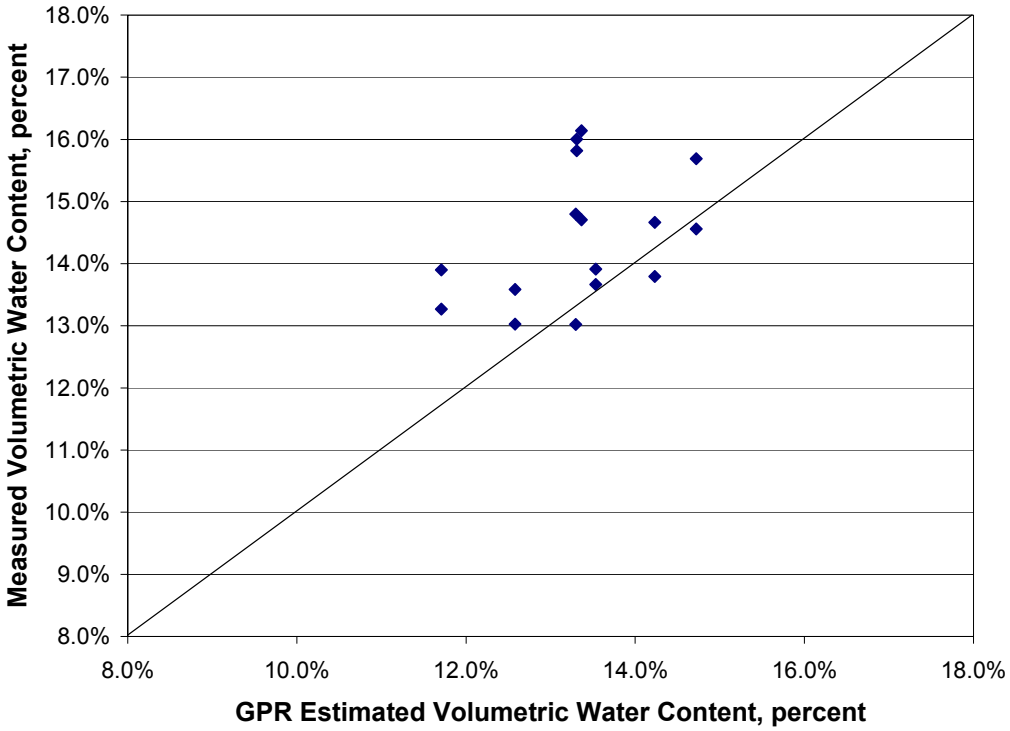


**Figure 12. Comparison of GPR and volumetric subbase moisture contents estimated from gravimetric moisture contents for Section 544.**

In general, GPR-derived estimates of volumetric water contents in the aggregate base were in the range of expected values. The average absolute error was less than 0.8 percent. The estimates for the aggregate subbase had an average absolute error of 0.9 percent. The inaccuracy of the GPR-derived estimates may be caused by varying thicknesses in the aggregate base and subbase or by uneven boundaries between the layers. Test pit data indicate that the aggregate subbase had varying thickness across the section.

Regardless of the inaccuracy of the estimates, the GPR technique can be an effective non-destructive method to estimate moisture contents of in-situ untreated base materials. Average absolute errors of ± 2 percent in estimated moisture contents are accurate enough for aggregate base and subbase materials.

## 3.2 Permanent Deformation Measurements

Permanent deformation data were gathered using the laser profilometer and multi-depth deflectometers (MDDs). The following sections summarize these data.

### 3.2.1 Surface Rutting Measured with the Laser Profilometer

Figure 13 shows accumulated average maximum rut depth for Section 544. A rapid rate of surface rutting was observed under the 40-kN trafficking load during the first load applications. Thereafter, no significant accumulation of surface rutting occurs under the 40-kN load. Surface rutting again increases under the 80- and 100-kN trafficking loads, with the rate of rutting decreasing with increasing load applications. Table 4 summarizes average rates of rutting for each of the three levels of traffic loading.

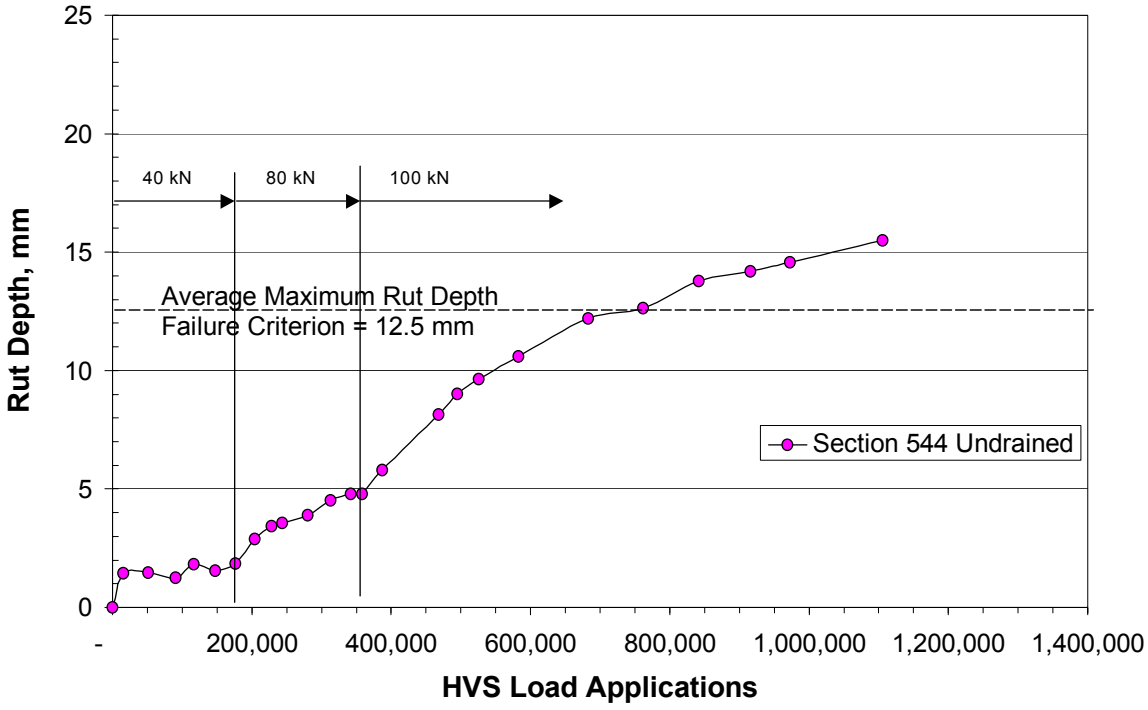


**Figure 13. Average maximum rut depth versus HVS load applications for Section 544.**

**Table 4 Average Rate of Rutting in Section 544**

| Trafficking Load | Rate of Rutting (mm/million load repetitions) |
|---|---|
| 40 kN | 10.5 |
| 80 kN | 18.7 |
| 100 kN | 13.5 |

Rut depth distributions at the end of the 40-, 80-, and 100-kN trafficking loads are shown in Figures 14a–14c. The center of the HVS wheelpath is marked as 0 mm transverse distance in the figures. The rut distribution is fairly uniform throughout the section with greater rutting localized around Stations 3 and 8.

### 3.2.2 In-depth Permanent Deformation

Figure 15 shows the permanent deformation recorded at several depths in the test section using the MDDs installed at Station 7 (refer to Figure 3 for the MDD depths in the pavement). Only deformations at the surface, at the top of the base, and at the top of the subbase were obtained since the lower two MDDs did not function properly.

Increase in permanent deformation with load applications is evident for all the layers under the 80- and 100-kN load. As in the surface rutting data, the rate of permanent deformation decreased with the number of load applications at the various depths. Permanent deformation development with HVS load applications are shown in Figure 16 for each pavement layer. (Note that it was not possible to separate permanent deformations occurring in the subbase and subgrade.)

Table 5 summarizes the average contributions to permanent deformation during loading of the asphalt concrete, aggregate base, and aggregate subbase/subgrade under 40-kN loading.

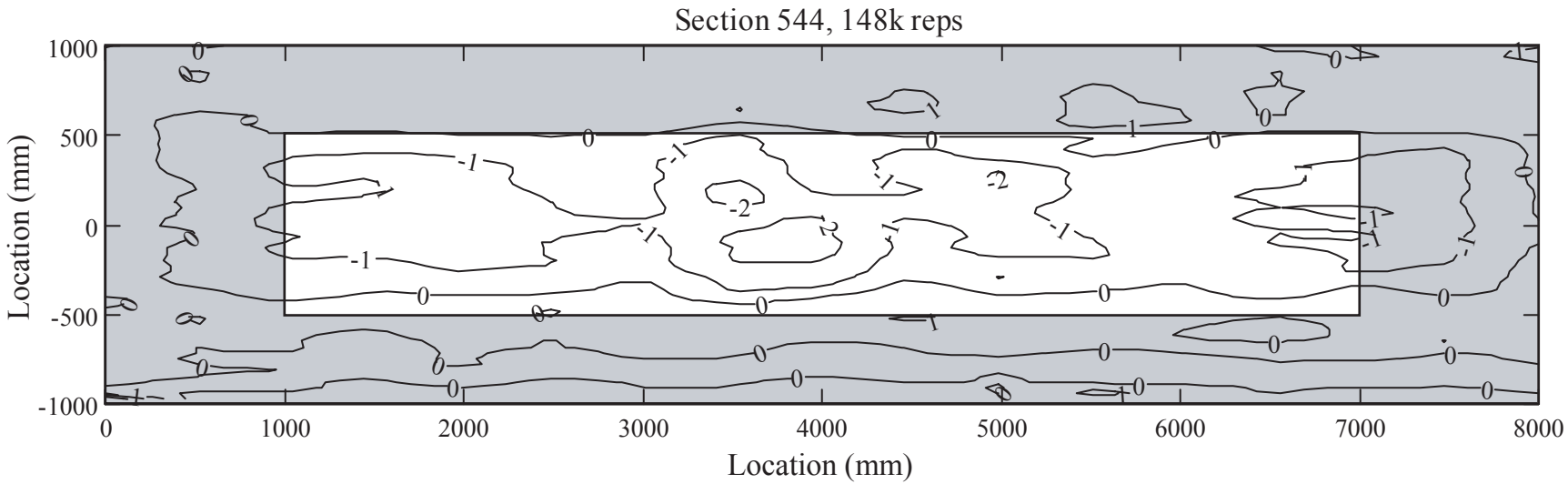


**Figure 14a. Section 544 surface profile after 147,583 load repetitions of the 40-kN load (mm).**



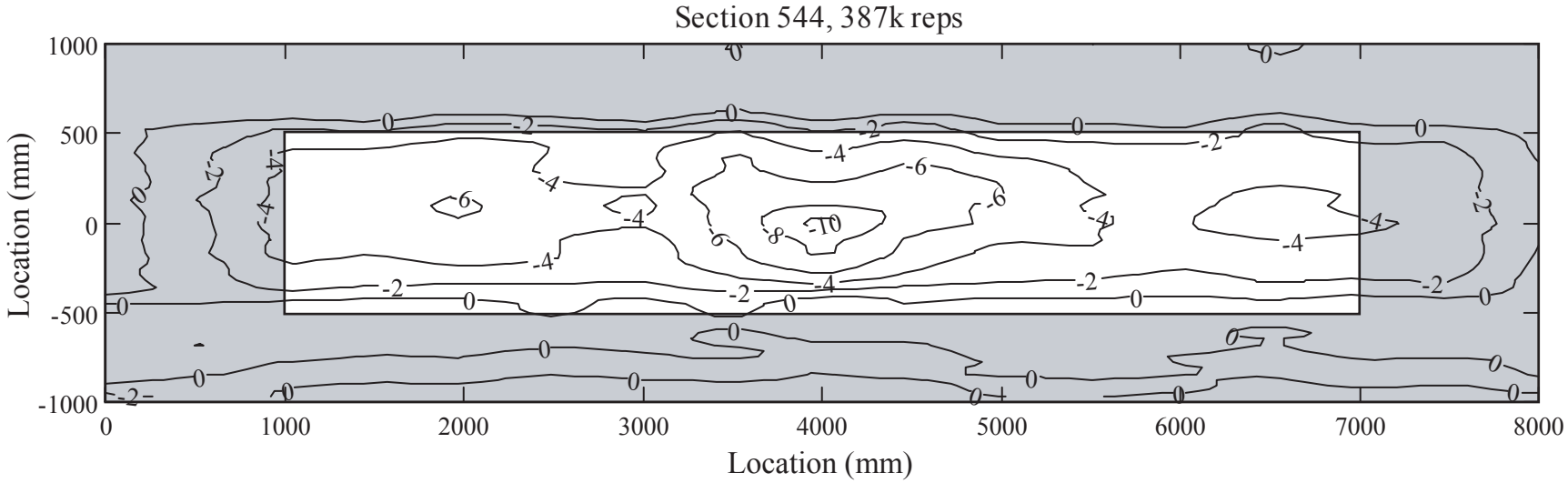


**Figure 14b. Section 544 surface profile after 387,027 load repetitions of the 80-kN load (mm).**

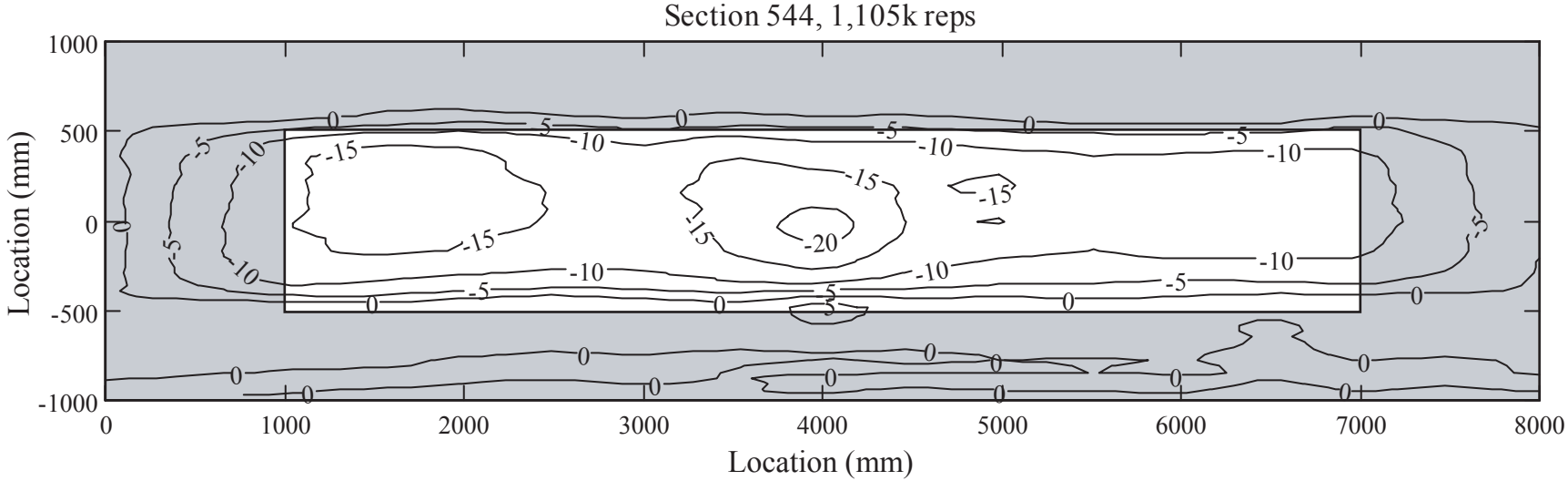


**Figure 14c. Section 544 surface profile after 1,105,123 load repetitions of the 100-kN load (mm).**

**Figure 14. Section 544 surface profiles at various stages of HVS trafficking (highlighted region indicates trafficked area minus the turnaround zones).**

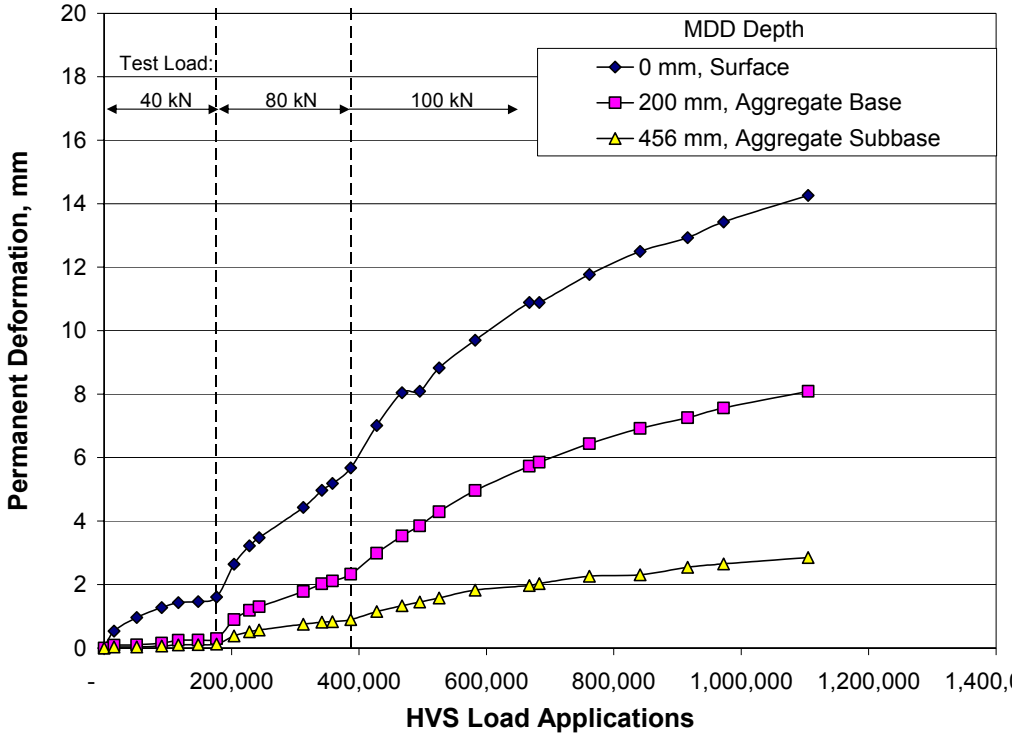


**Figure 15. In-depth permanent deformations with load repetitions, Section 544.**

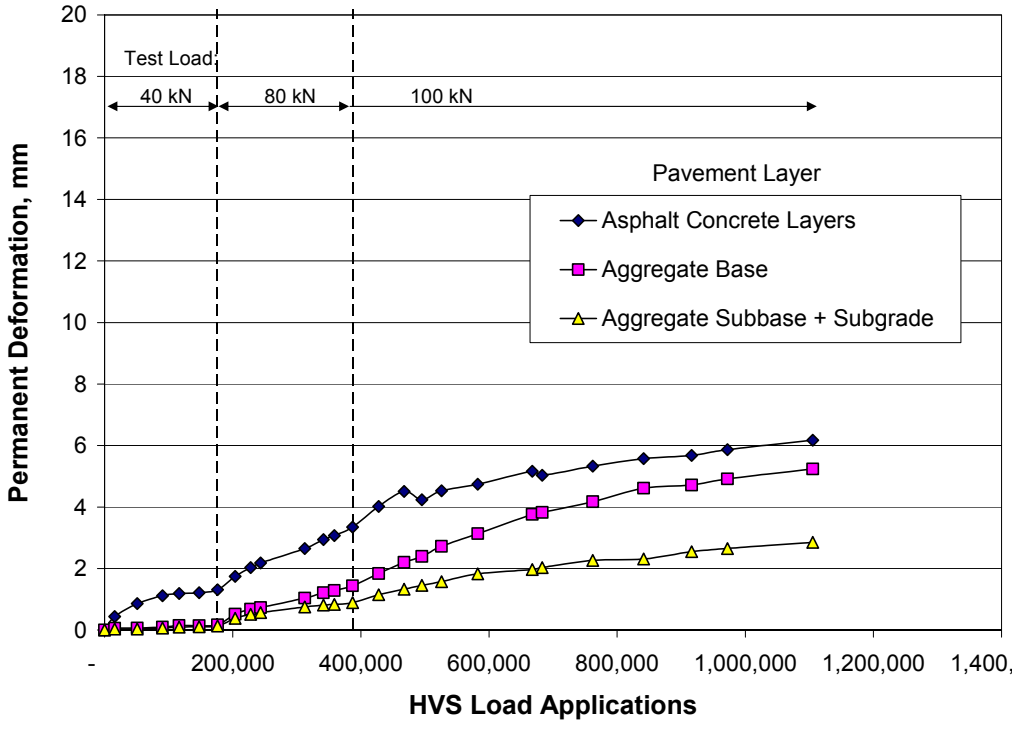


**Figure 16. Permanent deformation accumulation with load repetitions in the asphalt concrete, aggregate base, and subbase/subgrade layers, Section 544.**

**Table 5. Average Contribution of Each Pavement Layer to Surface Rutting**

| Pavement Component | Percent Contribution during Trafficking Load | | |
|---|---|---|---|
| | 40 kN | 80 kN | 100 kN |
| Asphalt Layers | 85 | 59 | 44 |
| Aggregate Base | 9 | 24 | 36 |
| Aggregate Subbase and Subgrade | 6 | 16 | 19 |

The majority of the permanent deformation under the 40-kN load, less than 2 mm, occurred in the asphalt concrete. Subsequently, under the 80- and 100-kN loading, the permanent deformation contributions of the underlying layers increased significantly due to the increased load stresses in these layers.

### 3.2.3 Comparison with Similar Sections Tested under Dry Conditions

Pavement Section 544 is similar to Section 501/517. This earlier section was tested first as Section 501 in the Goal 1 study with the aggregate base in a dry condition (the subgrade stiffness did change during loading due to seasonal precipitation). Following the Goal 1 study, a dense-graded asphalt concrete (DGAC) overlay was placed (versus the ARHM-GG overlay on Section 544 and tested as Section 517 with the base in essentially the same dry condition. A summary of loading applied to these tests is contained in Table 6.

**Table 6 HVS Traffic for Previous Sections Tested under Dry Conditions**

| Program | Number of Repetitions at Load | | |
|---|---|---|---|
| | 40 kN | 80 kN | 100 kN |
| Goal 1, Section 501 | 150,000 | 50,000 | 1,230,000 |
| Goal 3, Section 501/517 | 148,000 | 179,000 | 2,019,000 |

Figure 17 shows in-depth permanent deformation data obtained with the MDDs for Sections 501/517. Included in dashed lines are in-depth data for Section 544. The locations of the MDDs in Sections 501/517 are similar to those for Section 544. MDDs were located near the

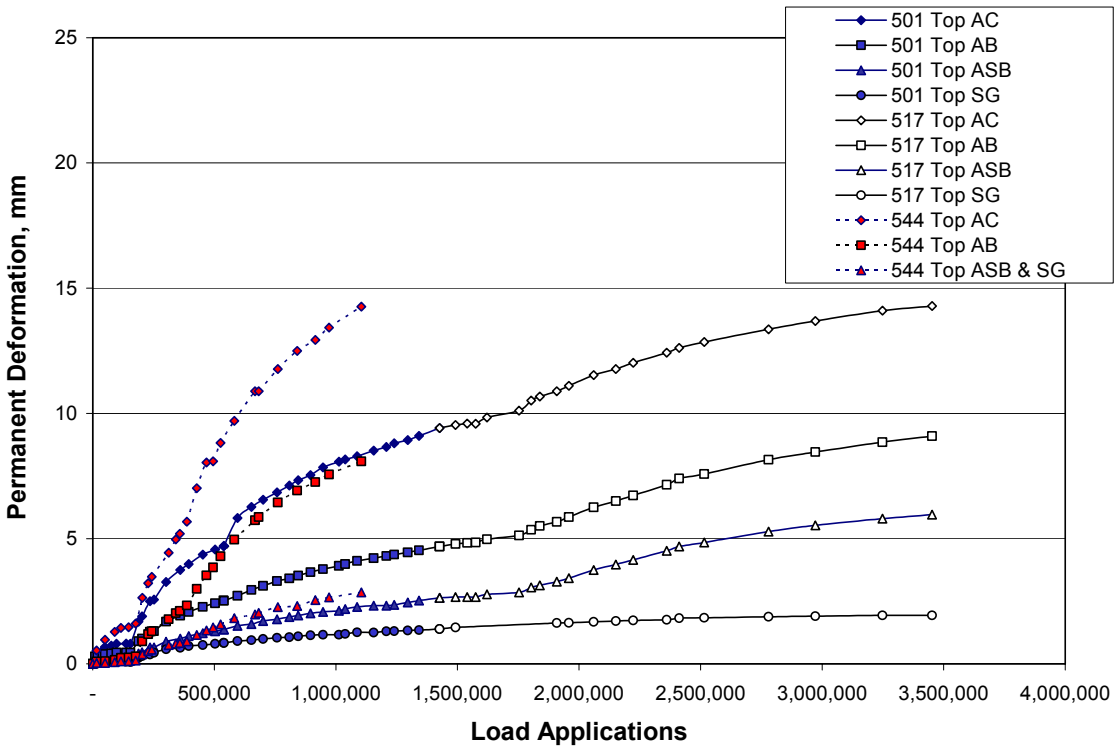


**Figure 17. Comparison of in-depth permanent deformations for dry and wet sections.**

surface of the pavement and at the top surface of the aggregate base, aggregate subbase, and subgrade. Differences in the rutting performance of the test sections are shown in this figure. The rate of permanent deformation with number of load applications was larger for Section 544 than for Section 501 at all in-depth modules, particularly for those near the surface and at the surface of the aggregate base. At the completion of HVS testing, surface permanent deformation was about 14 mm after 1.1 million load applications in Section 544 versus 9 mm after 1.4 million load applications in Section 501. In addition, permanent deformation on top of the aggregate base was about 8 mm in Section 544 versus less than 5 mm in Section 501. In Section 501/517 (Goal 3 HVS program), additional permanent deformation accumulated on the surface and top of the aggregate base similar to those of Section 544. However, the number of load applications during both Goal 1 and Goal 3 were more than twice those applied to Section 544. The results

indicate the significant difference in performance of a flexible pavement under conditions of dry and wet base conditions. Increased moisture content in the untreated aggregate base accelerates the rutting accumulation in this layer.

### 3.2.4 Comparison with Section 543 (Drained Section)

Section 543 was tested in the Goal 5 program with moisture conditions similar to those of Section 544. Section 543 differed from Section 544 in that it contained an ATPB layer between the asphalt concrete and the aggregate base. Results of testing Section 543 are presented in Reference (*6*). In-depth permanent deformations for Sections 543 are 544 are shown in Figure 18. MDD locations were similar for Sections 543 and 544.

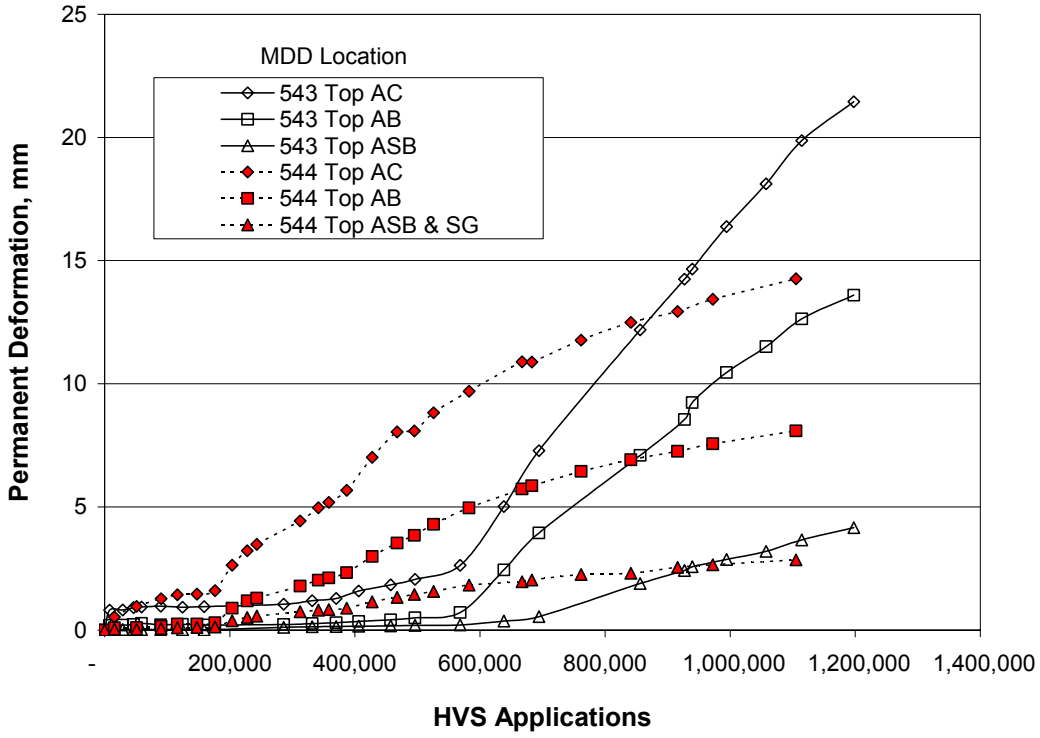


**Figure 18. Comparison of in-depth permanent deformations for drained and undrained sections under wet conditions.**

Differences in permanent deformation performance are evident in the two sections. Under the 40- and 80-kN loads, the permanent deformations in the asphalt bound (including ATPB) and aggregate base layers in Section 543 were lower than in Section 544. This suggests that for these load levels, the ATPB layer in Section 543 performed as a relatively intact layer and that water remained in the ATPB rather than migrating into the base. Under the 100-kN load, however, the ATPB failed due to stripping and fine particle contamination producing increasing rates of permanent deformation with the number of load applications.

In Section 544, permanent deformations accumulated at a decreasing rate with load applications. The relatively better performance of the aggregate base in Section 544 was likely due to the difference in stress state as compared to that in Section 543 because of the deteriorated condition of the ATPB. In addition, the increase in moisture content of the base of Section 543 due to the reduced permeability of the ATPB contributed to the performance differences.

The relative performance of Sections 544 and 543 illustrate the importance of maintaining the ATPB in an intact condition. The rapid increase in permanent deformation in Section 543 when the 100-kN loads were applied can be attributed to the deterioration of the ATPB and its becoming clogged with fines. This performance difference emphasizes these important points:

1. If ATPB is used, it should be designed to prevent stripping on the assumption that the drainage system could lose its effectiveness.
2. Proper maintenance of the drainage system in imperative.
3. A filter fabric should be placed between the untreated base and the ATPB to prevent migration of fines into the ATPB. A prime coat or the aggregate base is insufficient as demonstrated by the performance of Section 543.

## 3.3 Elastic Deflections

Elastic deflections in the pavement sections were measured with the Road Surface Deflectometer (RSD) and MDDs. Surface and in-depth deflection data presented in the following sections are peak values obtained from the deflection basins.

### 3.3.1 Surface Deflection Data

Surface elastic deflections were monitored using the RSD along the section centerline at Stations 4, 6, 8, 10, and 12 under the 40-, 80-, and 100-kN test loads. Figure 19 shows average deflection data for the three test loads. Elastic deflections significantly increased in the section under the 80-kN trafficking load; only a slight increase in these deflections was observed under the 100-kN trafficking load under all test loads.

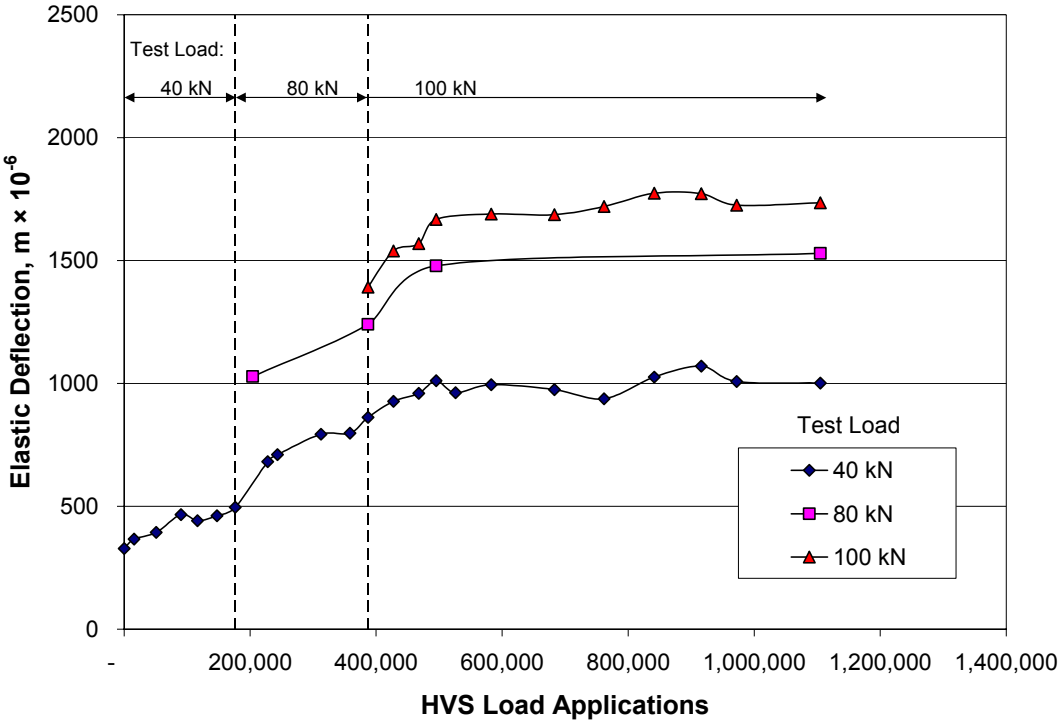


**Figure 19. RSD deflections for Section 544.**

It is believed that a significant amount of damage—cracks initiating at the bottom of the asphalt concrete—occurred under the 80-kN load and propagated through the asphalt concrete under the 80- and 100-kN loads. This would account, to some extent, for the relative small increase in deflections when the 100-kN load was applied.

Figure 20 shows RSD deflections along Section 544 obtained at the completion of HVS testing. The data indicate that the elastic response of the section is fairly uniform throughout. Coefficients of variance for the measured elastic deflections at 40-, 80-, and 100-kN test loads were 8, 6, and 3 percent, respectively.

### 3.3.2 In-depth Pavement Deflections

In-depth elastic deflection data for the 40-, 80-, and 100-kN test loads are presented in Figures 21, 22, and 23. Increases in elastic deflections in all layers were observed with increased

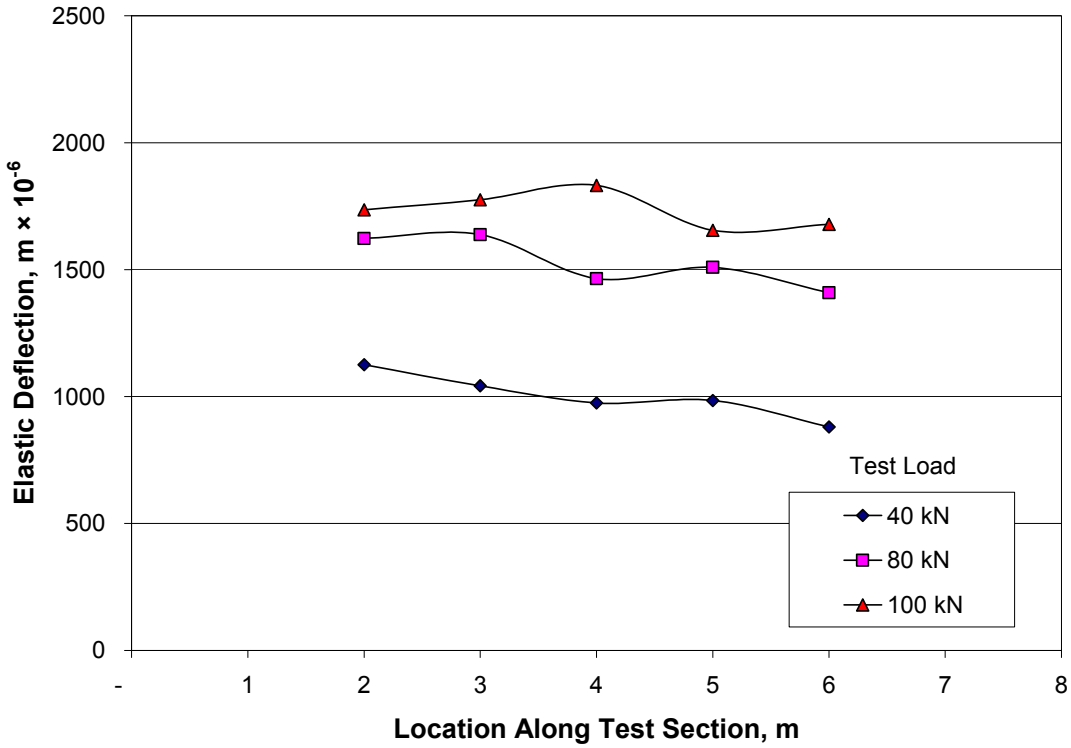


**Figure 20. RSD results at the completion of HVS trafficking, 1,105,123 load applications.**

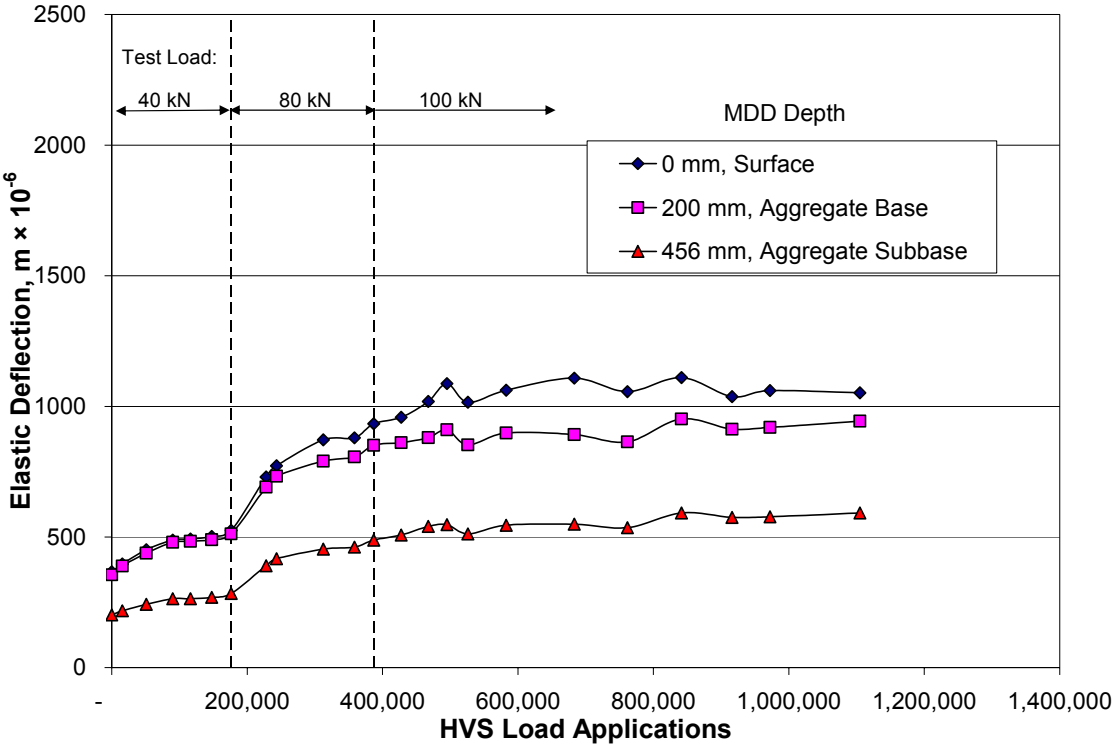


**Figure 21. In-depth elastic deflections under 40-kN test load, MDD 7.**

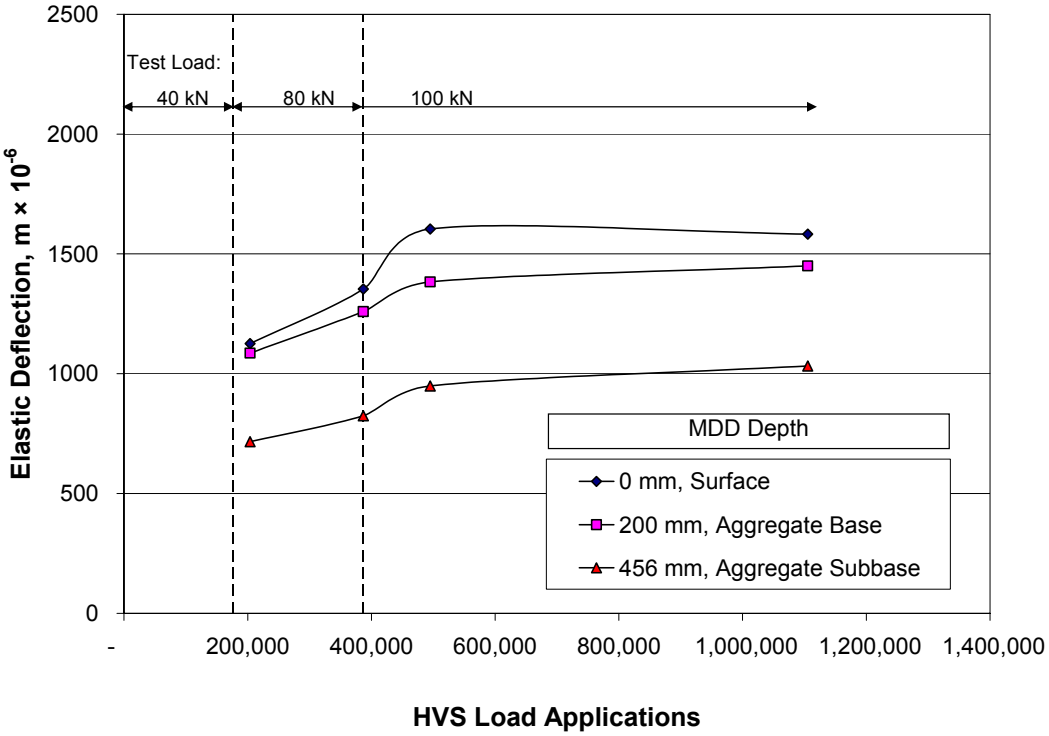


**Figure 22. In-depth elastic deflections under 80-kN test load, MDD 7.**

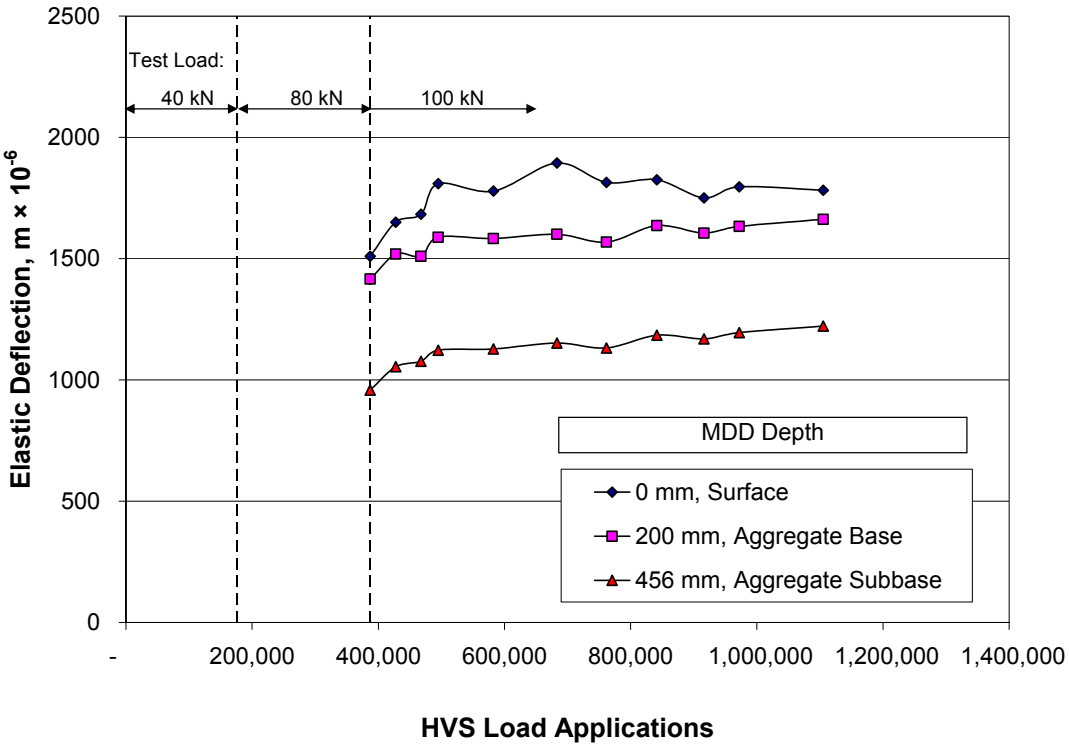


**Figure 23. In-depth elastic deflections under 100-kN test load, MDD 7.**

HVS trafficking under all test loads. The data indicate that the unbound layers yielded the highest elastic deflections. Deflections reached approximately constant values at about 470,000 HVS load applications for all test loads. Discussion included in the previous section for the RSD values apply to the in-depth deflections as well.

Elastic deflections for each pavement layer during HVS testing are presented in Figures 24, 25, and 26. The aggregate subbase and subgrade exhibited, proportionately, the largest deflections followed by the aggregate base and the asphalt bound layers (Table 7). The increased subbase/subgrade elastic deflections can be attributed to the increase in subgrade moisture content during HVS trafficking resulting from the winter precipitation, Figure 7. The change in relative contribution to deflection of each of the layers with increase in load demonstrates the stress dependency on load level, particularly for the untreated layers.

**Table 7 Average Cumulative Contribution of Pavement Layers to Surface Elastic Deflection**

| Pavement Layer | Percent Contribution of Layer to Surface Elastic Deflection at Trafficking Load/Test Load Combination | | | | | |
|---|---|---|---|---|---|---|
| | 40 kN/ 40 kN | 80 kN/ 40kN | 80 kN/ 80 kN | 100 kN/ 40 kN | 100 kN/ 80 kN | 100 kN/ 100 kN |
| Asphalt Layer | 2 | 7 | 5 | 14 | 11 | 10 |
| Aggregate Base | 44 | 40 | 33 | 33 | 27 | 27 |
| Aggregate Subbase and Subgrade | 54 | 53 | 62 | 53 | 62 | 64 |

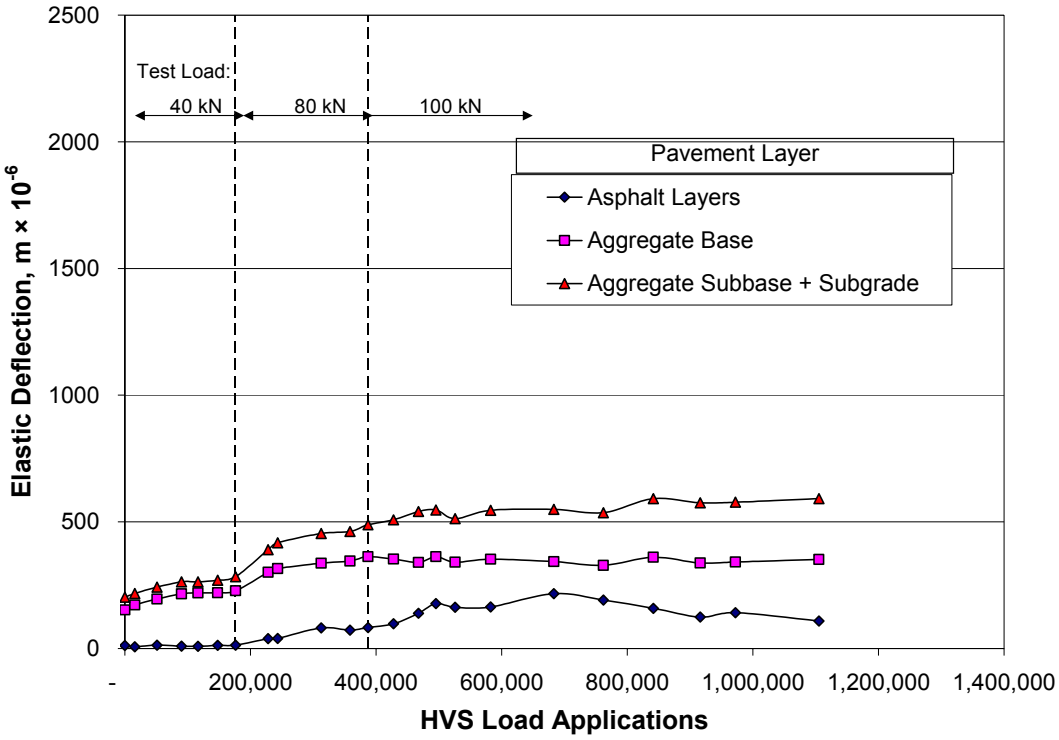


**Figure 24. Layer elastic deflections under 40-kN test load.**

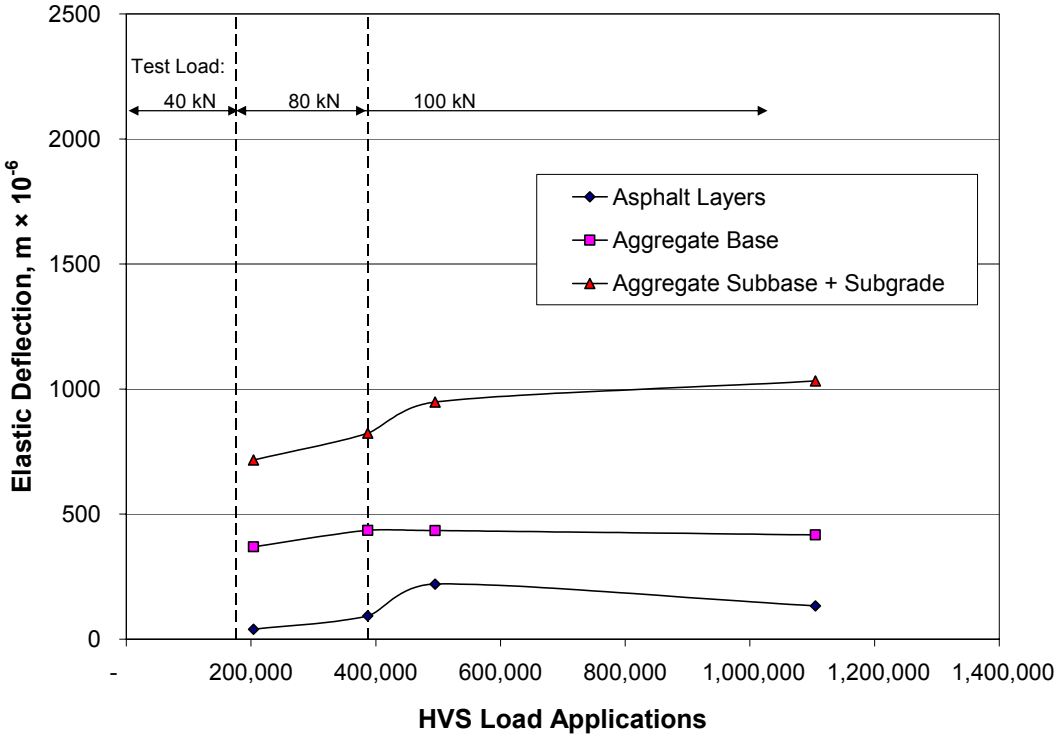


**Figure 25. Layer elastic deflections under 80-kN test load.**

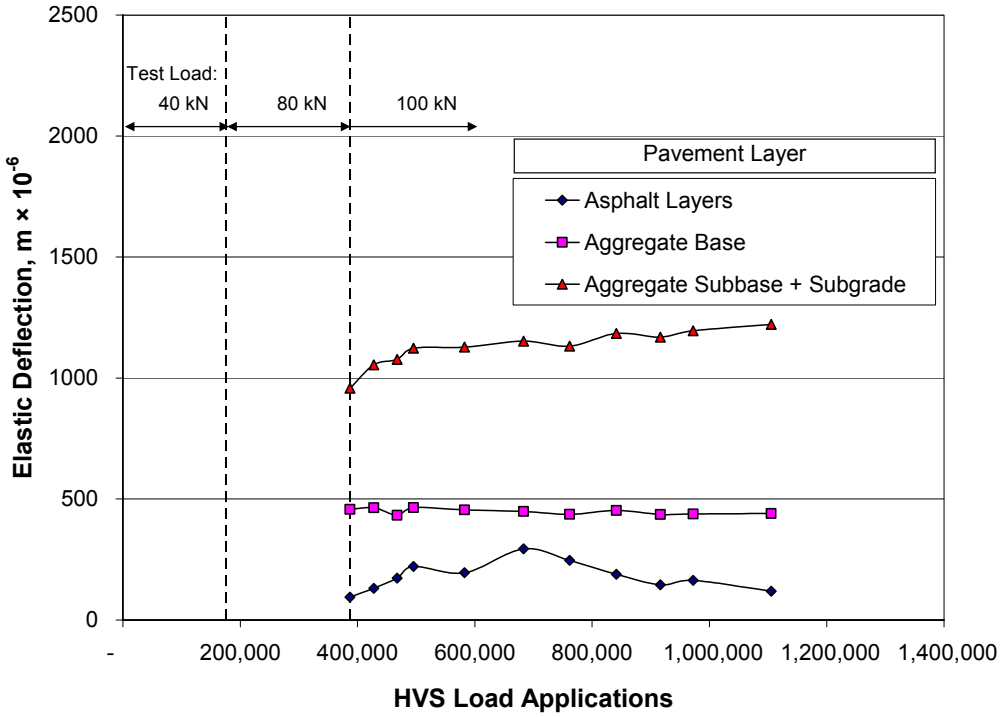


**Figure 26. Layer elastic deflections under 100-kN test load.**

Deflection data as profiles of deflections with respect to pavement depth are shown in Figure 27. The reduction in slop of the deflection profile in the upper portion of the pavement structure results from fatigue cracking in the asphalt-bound layers due to HVS trafficking and to a change in the state of stress as well as increased moisture content in the aggregate base.

### 3.3.3 Comparison with Section 501 Tested under Dry Conditions

Pavement Section 501, similar to Section 544, was tested earlier in the dry condition with the HVS. Comparative information for the two sections was presented in Section 3.2.3. Figure 28 shows in-depth MDD elastic deflections for the 40-kN test load for Section 501. Included in dashed lines are in-depth data for Section 544.

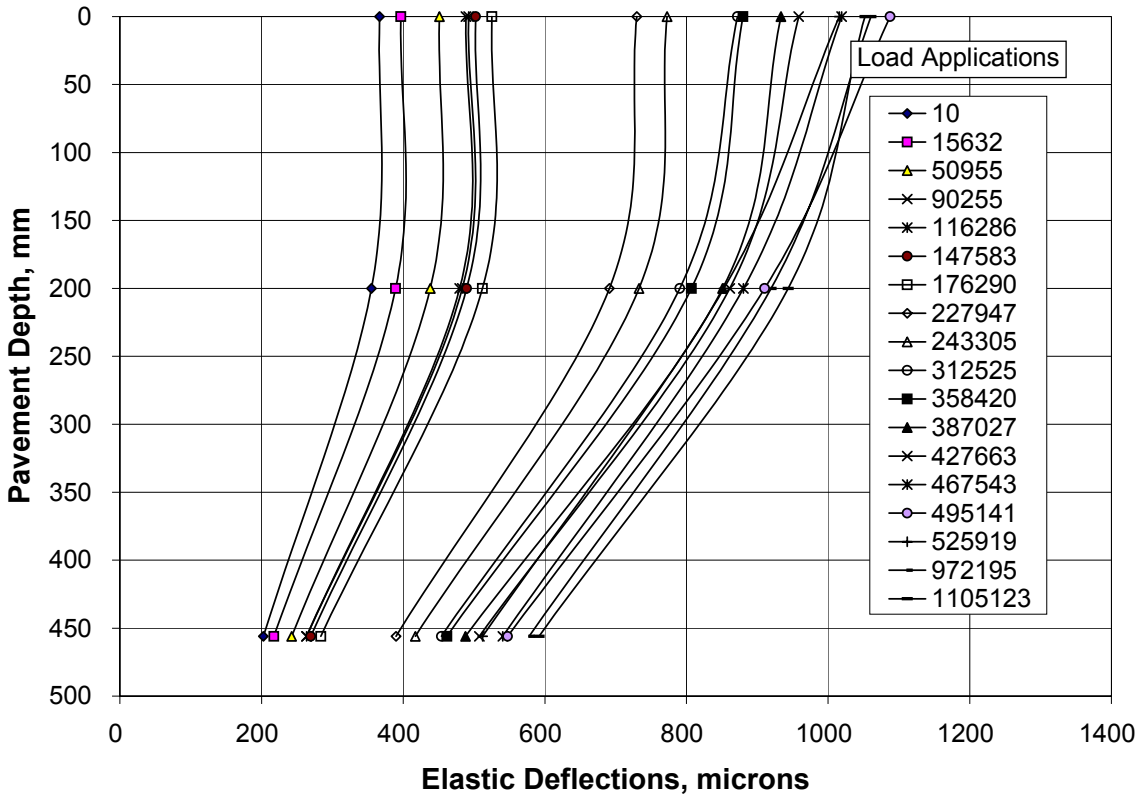


**Figure 27. Profile of elastic deflections with respect to pavement depth for the 40-kN test load.**

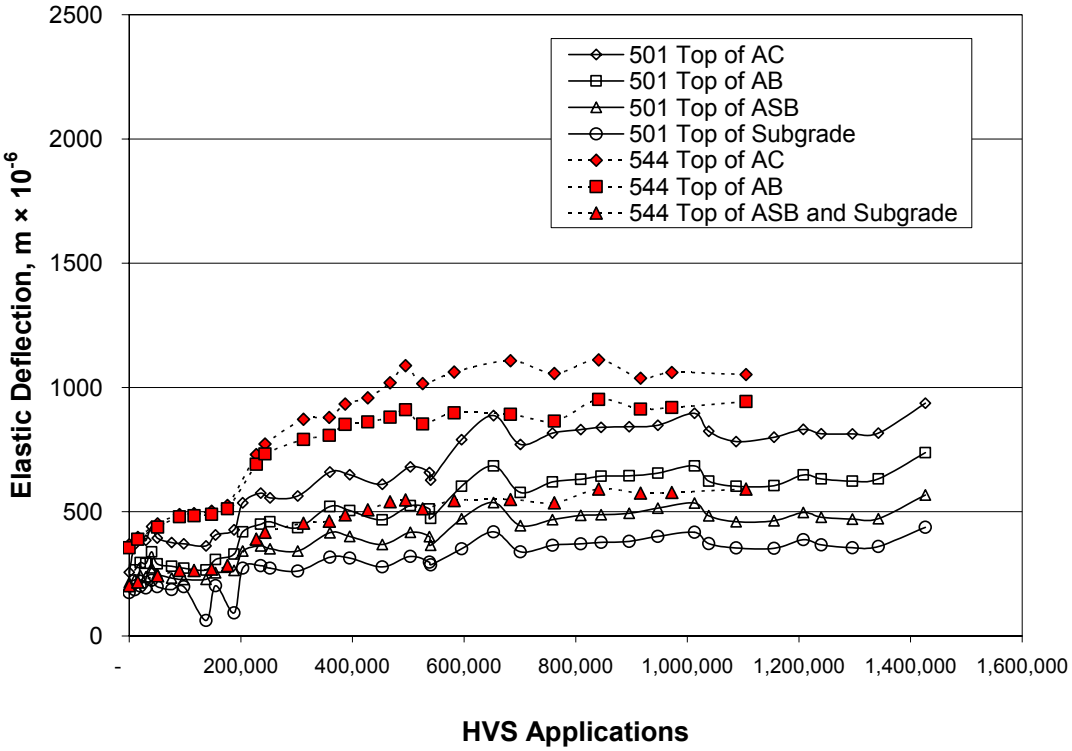


**Figure 28. Comparative performance of Sections 501 and 544, elastic deflections versus HVS load applications; 40-kN test load.**

Elastic deflections at the beginning of the test were similar for both sections indicating similar pavement responses. However, as the number of load applications increased, elastic deflections increased faster in Section 544 than in Section 501. Elastic deflections in Section 544 leveled off at about 1065 microns for elastic deflections measured close to the surface, and at about 905 microns for the top of the aggregate base. In Section 501, elastic deflections rapidly leveled off during the three trafficking loads. Surface and top of the aggregate base deflections leveled off at about 825 microns and 634 microns, respectively. The elastic deflections at the surface of the AC and top of the aggregate base in Section 544 were about 29 and 42 percent higher, respectively, than those in Section 501. Elastic deflections on top of the subbase were about 15 percent higher in Section 544 than in Section 501. Based on the results for both sections, the largest increase in layer deflection was in the aggregate base mainly due to an

increase in moisture content and change in stress state due to cracking in the asphalt concrete layers.

### 3.3.4 Comparison with Section 543 (Drained)

In depth elastic deflections obtained under the 40-kN test load for Section 543 are shown in Figure 29. Included as dashed lines are in-depth data for Section 544. In-depth elastic deflections at the beginning were higher for Section 544 than for Section 543. Thereafter, deflections in Section 544 increased faster with the number of load applications. During the 40- and 80-kN trafficking loads, surface deflections were significantly lower in Section 543, indicating that the structural integrity of the ATPB was maintained. However, under the 100-kN

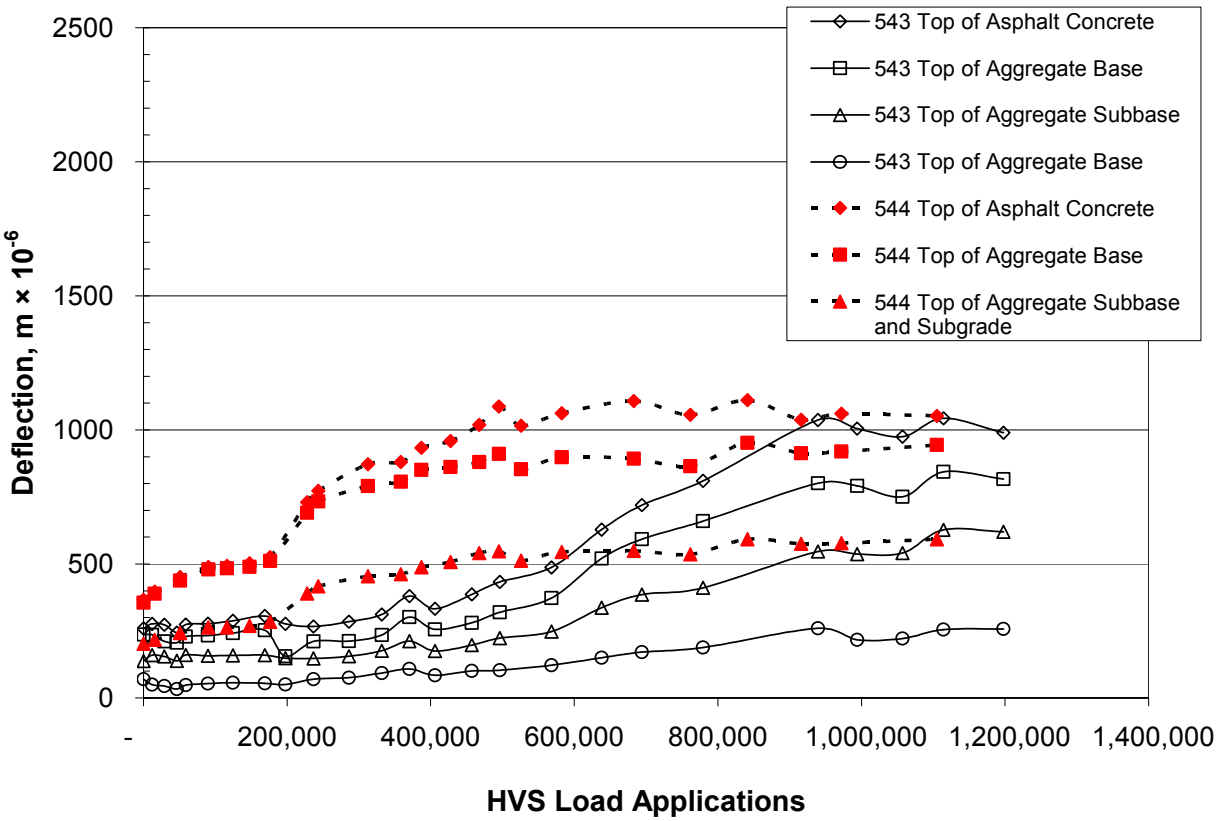


**Figure 29. Comparison of elastic deflections from Sections 543 and 544, 40 kN load.**

load, elastic deflections in Section 543 increased significantly as a result of stripping in the ATPB and reached levels similar to those of Section 544. Once the ATPB stripped, it exhibited behavior similar to that of an aggregate base. Elastic deflections on top of the aggregate base were about 12 percent lower in Section 543 at the end of HVS testing because of the lower vertical stresses resulting from the added 75 mm of stripped ATPB.

### 3.3.5 Backcalculated Moduli from In-depth Elastic Deflections

Moduli of the pavement layers were backcalculated from the in-depth elastic deflection basins measured with the MDDs. Calculated deflections for the same positions were determined using the Odemark procedure for a four-layer system represented by the asphalt bound layers, aggregate base layer, aggregate subbase, and a non-linear subgrade.(*7*)

Figure 30 summarizes the backcalculated moduli from the MDD data obtained for the 100-kN test load. Backcalculated moduli for the 40- and 80-kN test loads yielded spurious results and are not included in Figure 30. It will be observed that a decrease in the modulus of the asphalt bound layers with HVS load applications was obtained. This reduction is likely due to the observed cracking in the pavement. Reduction in the modulus of the asphalt concrete layer during the 100-kN loading was about 40 percent (from 844 MPa down to 515 MPa) since much of the damage occurred under the 80-kN test load, as noted earlier. For the untreated layers, the backcalculated moduli of the aggregate base were similar to those for the aggregate subbase and subgrade. The low moduli in the untreated aggregate base are likely the result of an increase in the moisture content and change in stress state due to cracking of the asphalt concrete. Backcalculated moduli for the subgrade show little variation during the 100-kN loading. It will be noted that the moduli of the aggregate base and subgrade are similar and the subbase moduli are, on average, slightly less than those of the subgrade. These values are undoubtedly a

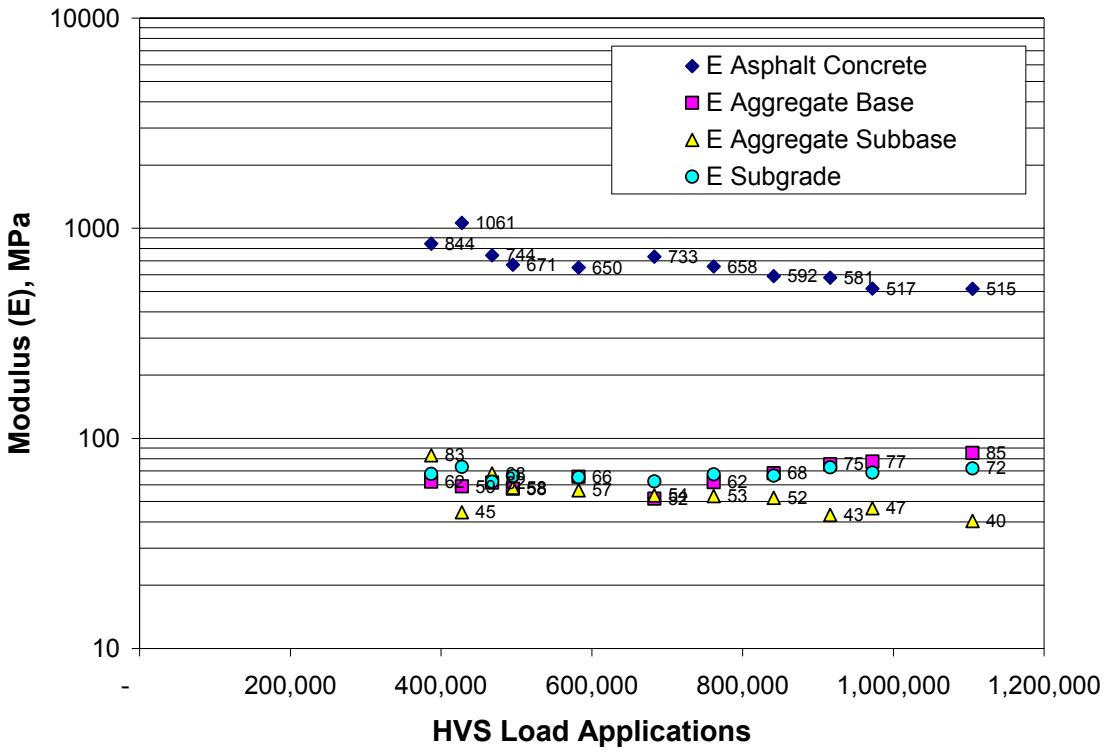


**Figure 30. Layer moduli backcalculated from MDD deflections for Section 544.**

function of the complex stress states and the non-linear response characteristics of these untreated materials.

Figure 31 shows backcalculated moduli for the pavement layers of Section 543. Comparison of the moduli for Sections 543 and 544 indicates that the layer moduli of the asphalt-bound layers showed a larger stiffness reduction under the 100-kN loading than in Section 544 (about 80 percent versus 40 percent) because of the stripping which took place in the ATPB. It is also interesting to observe that in the latter part of the 100-kN loading the backcalculated moduli of the untreated materials are similar in the two sections.

These results illustrate the useful information that the backcalculation process can provide to assist in the analysis of pavement performance. In addition, the results illustrate the usefulness of estimating moduli based on MDD deflection basins since the analyses yielded similar untreated layer moduli for the two sections as would be anticipated.

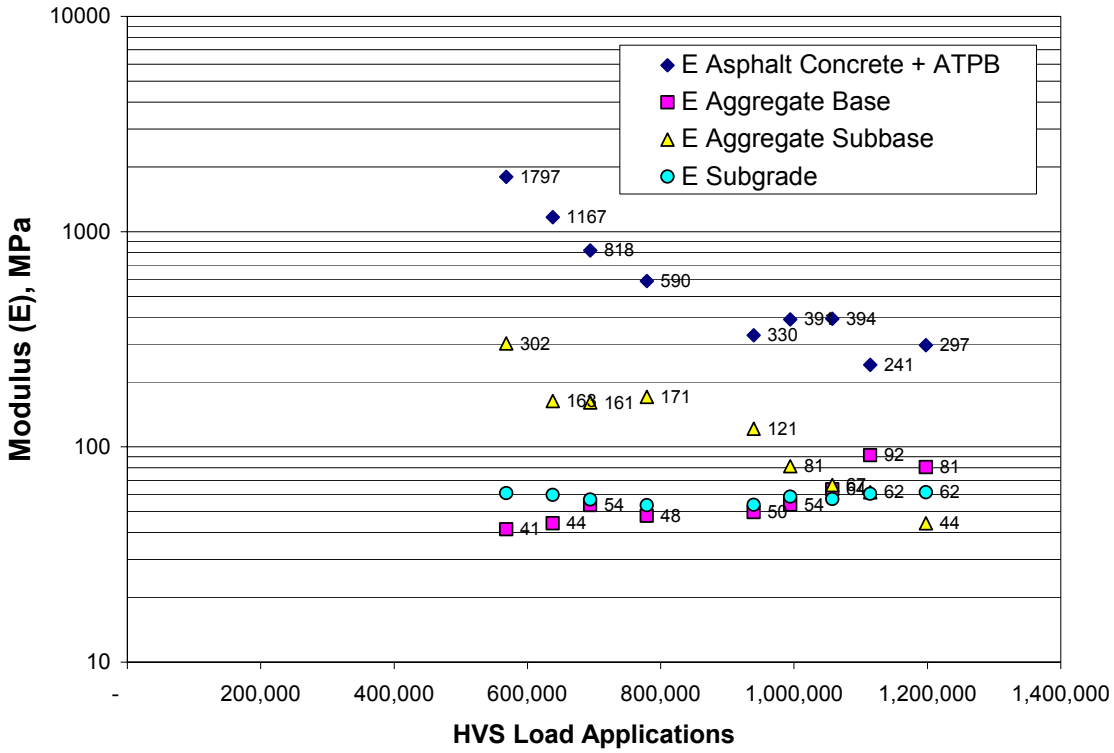


**Figure 31. Backcalculated moduli for Section 543.**

### 3.4 Crack Length Progression

Figure 32 shows the cracks detected during HVS trafficking after 667,477; 930,145; and 1,090,441 load applications. The observed cracks were predominantly transverse hairline cracks and were sometimes difficult to detect visually. The typical widest crack widths were approximately 0.2 mm. These hairline cracks did not spall or increase significantly in width during HVS trafficking. The lack of crack deterioration is due to lack of mineral particles on the pavement surface that otherwise would intrude into the cracks creating stresses around the edges of cracks when they open or close due to traffic and temperature changes. The HVS temperature control box, which limited daily expansion and contraction of the asphalt, further mitigated crack deterioration.

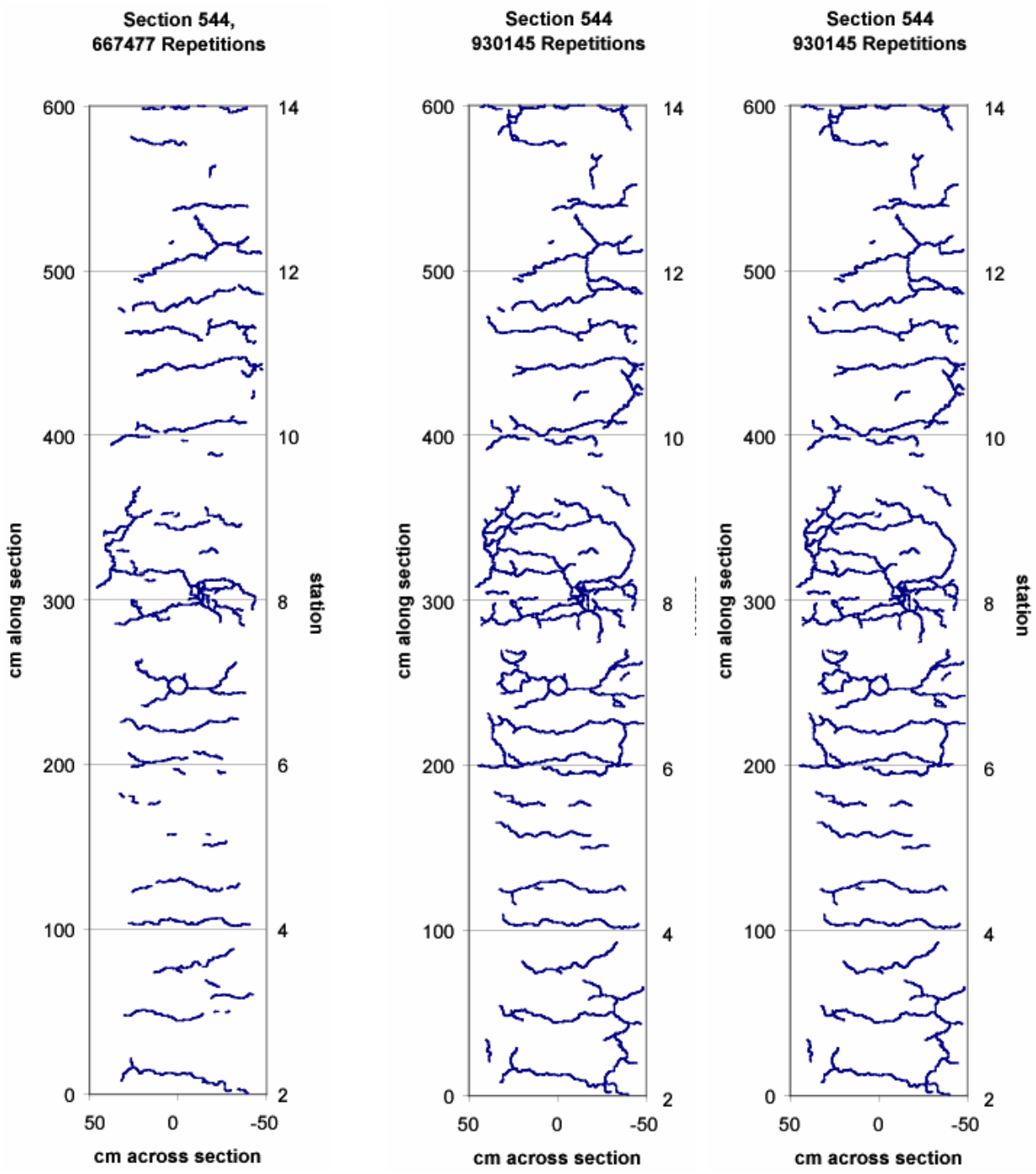


**Figure 32. Surface crack schematics for Section 544.**

Figure 33 shows the crack distribution along the test section at the completion of HVS trafficking. Crack densities were in the range of 5 and 10 $m/m^2$ at the end of HVS testing; these crack densities exceeded the failure criterion of 2.5 $m/m^2$.

Figure 34 shows measured total surface crack length and crack density on Section 544 versus HVS load applications. The data show the rapid increase of surface cracks with load applications. All the surface cracks appeared under the 100-kN trafficking load.

As previously mentioned, it is hypothesized that most of the damage (crack initiation) occurred under the 80-kN trafficking load. As seen in Figure 19, for example, elastic deflections stopped increasing at the beginning of the 100-kN trafficking load. However, crack propagation took place primarily under the 100-kN trafficking load, as indicated by the continued increase in the appearance of surface cracks well into the period of 100-kN trafficking.

## 3.5 Falling Weight Deflectometer (FWD) Testing

FWD testing was conducted on Section 544 along the centerline of the pavement at 1-foot intervals to evaluate the structural integrity of the pavement and to estimate moduli of the layers from the measured deflections. Three load levels (20, 40, and 60 kN) were applied for assessing non-linearities in the pavement response. The loads were applied to the pavement by a 300-mm diameter plate. FWD data were collected during stages 1, 2, and 4; FWD data were not collected during Stage 3 since it would have required moving the HVS off of the test section to accommodate the FWD equipment.

### 3.5.1 FWD Normalized Deflections

Figure 35 summarizes elastic deflections measured under the FWD load plate normalized to a 40-kN load (termed $D_0$) for the three test stages during which FWD testing was conducted.

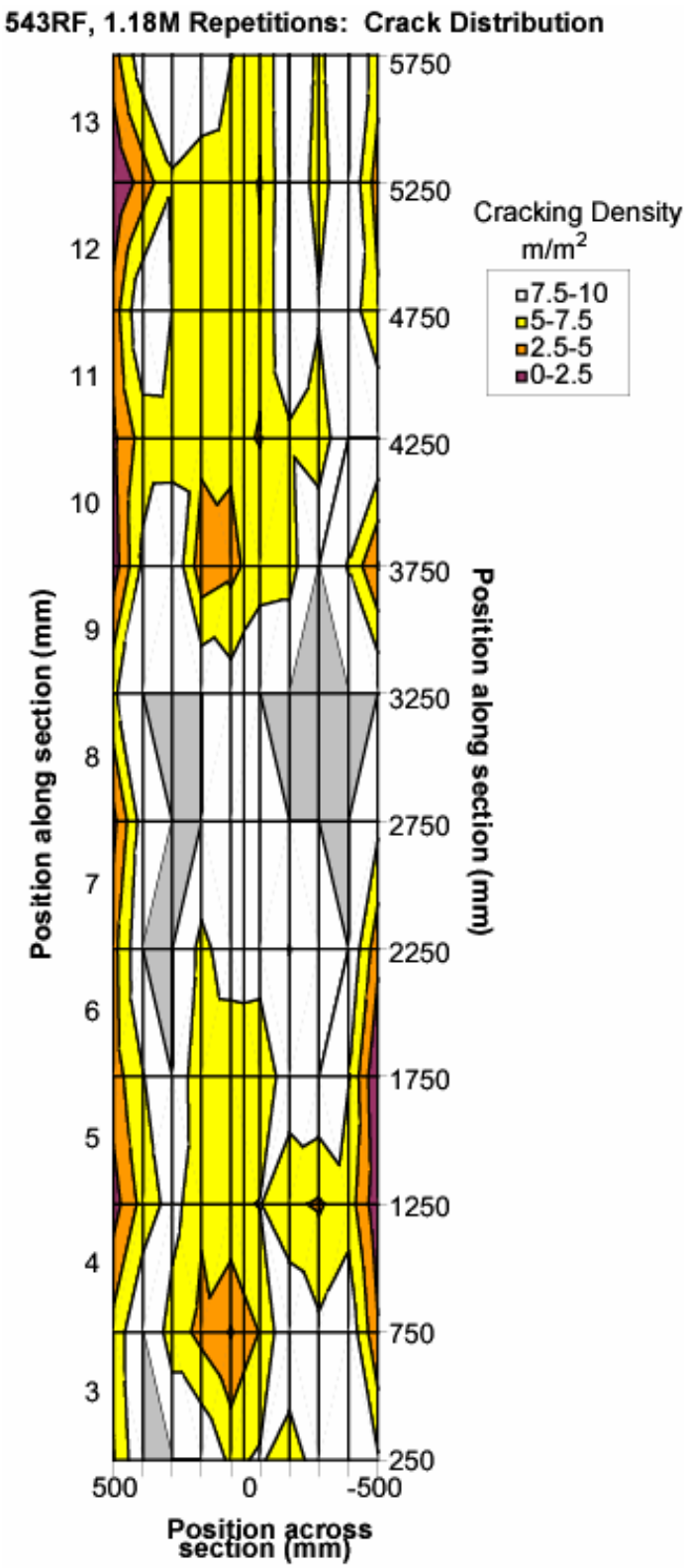


**Figure 33. Contour plot of cracking density on Section 544 at the completion of HVS trafficking.**

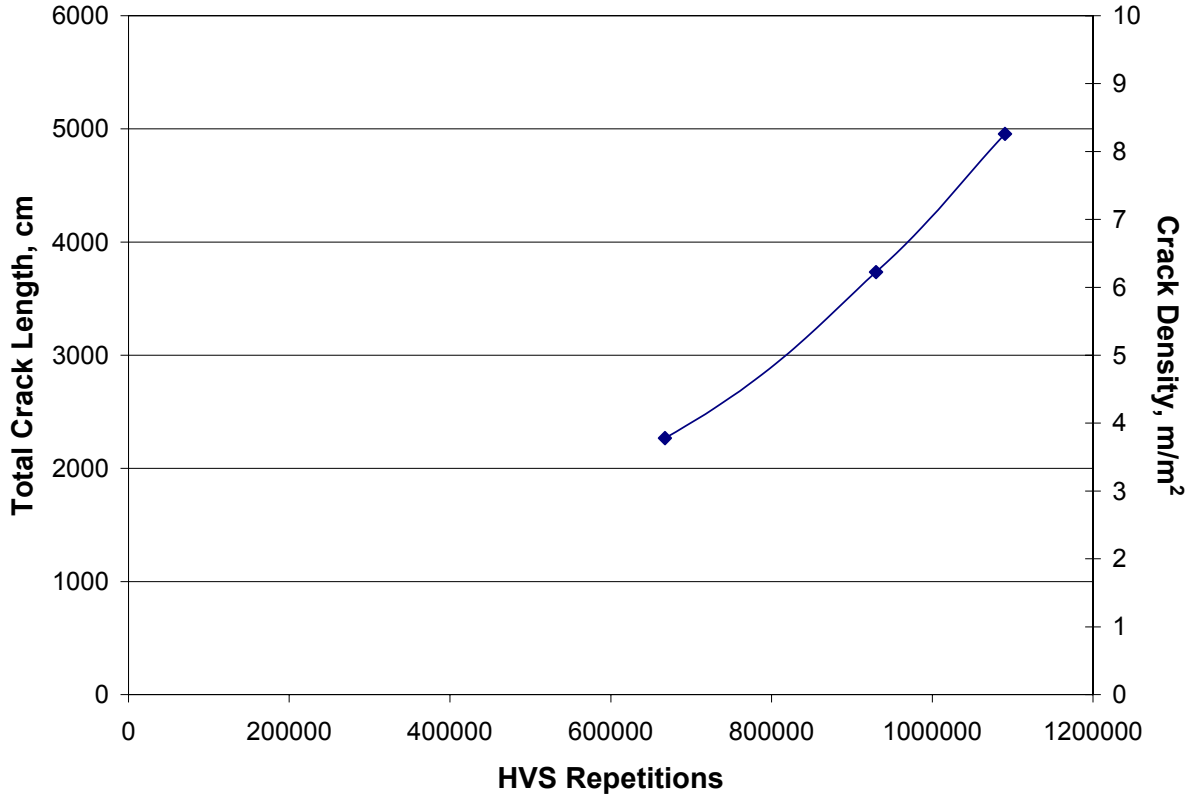


**Figure 34. Crack length progression in Section 544.**

The figure shows no significant variation in $D_0$ deflections between Stage 1 (no water infiltration) and Stage 2 (water infiltration). However, a significant increase in deflections was observed during Stage 4. Table 8 summarizes average normalized deflections obtained during the three periods of FWD testing. It will be noted that in Stage 4 (after HVS testing), deflections were approximately three times those measured in Stages 1 and 2.

Interestingly, for the FWD tests conducted several weeks after the final HVS testing, some reduction in deflections was observed. This reduction could in part by due to a decrease in moisture content in the aggregate base since water infiltration was stopped at the conclusion of the HVS testing (Stage 3). One might argue that some "healing" may have also occurred in the asphalt concrete. Experience in previous HVS tests has been that the so-called healing

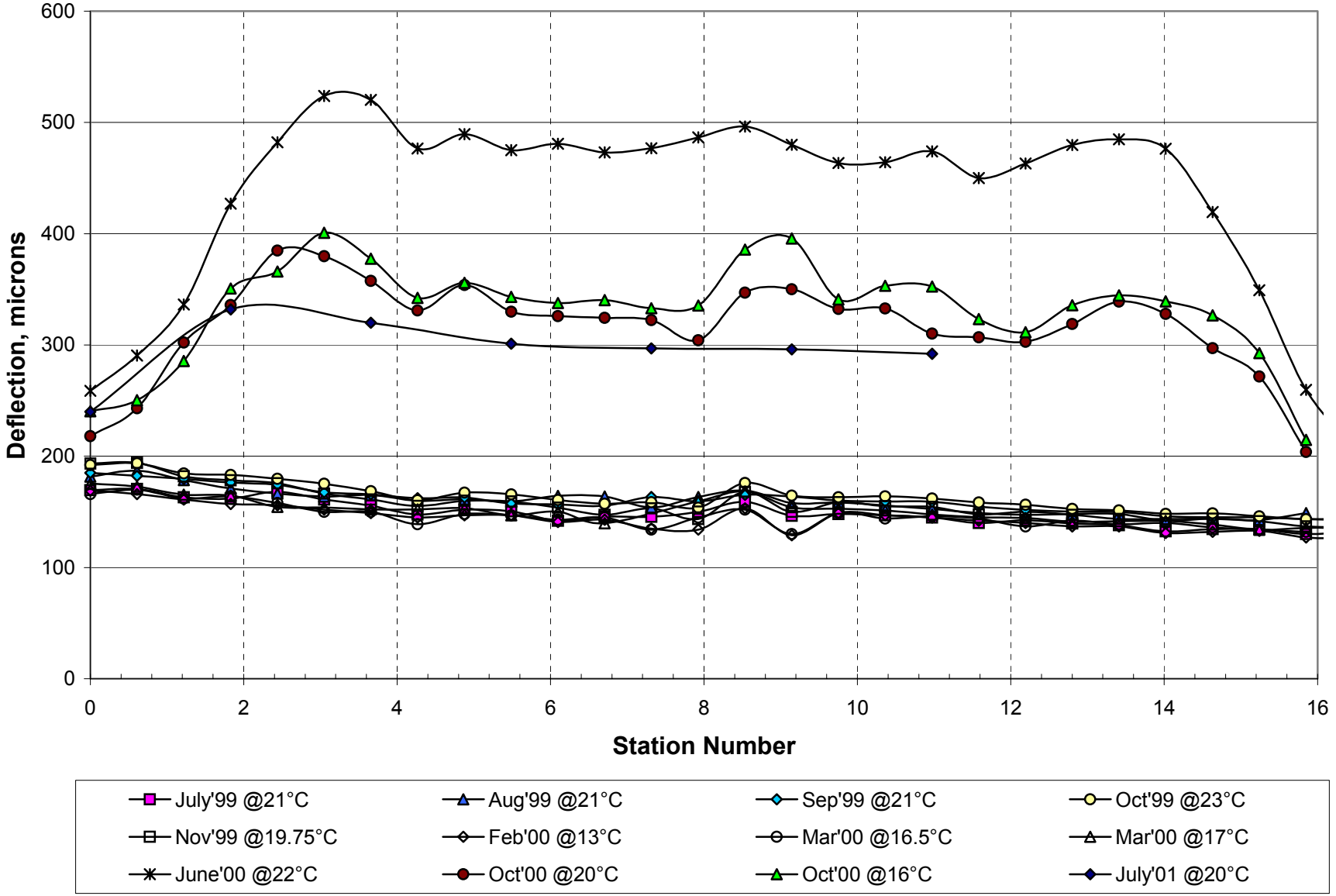


**Figure 35. FWD deflections normalized to a 40-kN load for Stages 1, 2, and 4.**

**Table 8 D1 Deflections Normalized to a 40-kN load.**

| Test Date | | Average Deflections, microns | Standard Deviation, microns | Average Air Temperature, ºC |
|---|---|---|---|---|
| Stage 1 | July'99 | 146.7 | 7.1 | 18.6 |
| Stage 2 | Aug'99 | 157.0 | 7.5 | 21.0 |
| | Sep'99 | 158.5 | 6.0 | 21.4 |
| | Oct'99 | 161.3 | 7.5 | 23.0 |
| | Nov'99 | 153.6 | 7.4 | 21.0 |
| | Feb'00 | 142.3 | 7.0 | 13.0 |
| | Mar'00 | 143.4 | 5.8 | 16.5 |
| | Mar'00 | 149.8 | 7.2 | 17.0 |
| Stage 3 | June'00 | 480.7 | 18.0 | 22.0 |
| | Oct'00 | 331.4 | 19.9 | 20.0 |
| | Oct'00 | 349.9 | 23.9 | 16.0 |
| | July'01 | 301.2 | 11.0 | 20.0 |

phenomenon is temporary. If HVS testing is resumed after a period of no loading, within relatively few repetitions, the deflection return to the levels measured prior to stopping the HVS loading.

### 3.5.2 Backcalculated Moduli from FWD Deflections

Moduli were backcalculated from FWD deflections obtained from the three target loads for a three layer system: asphalt bound layers (AC), aggregate base layers (AB), and the subgrade (SG). This system was selected for simplicity. The backcalculation process was conducted using the program ELMOD 4.5, which uses the Odemark-Boussinesq method and assumes a non-linear subgrade. Table 9 summarizes the layers and thicknesses for the two cases considered.

**Table 9 Summary of Layers and Thicknesses Considered for Backcalculation**

| Layer | Thickness, mm |
|---|---|
| AC (asphalt bound layers) | 200 |
| AB (aggregate base + aggregate subbase) | 532 |
| SG (subgrade) | assumed infinite |

Results of the backcalculation process are presented in Figure 36 through 38 and include moduli determined from the three load levels used during FWD testing. Also presented in the figures are results of the backcalculation process using the MDD deflections (Stage 3) for the 100-kN dual wheel load.

Figure 36 shows the modulus of the asphalt concrete layers. The modulus of the combined asphalt concrete layers range from 5000 to 7500 MPa and variations seem follow the estimated pavement temperatures. Pavement temperatures were estimated from air temperatures using the BELLS equation.(*8*) Asphalt concrete moduli after HVS testing were about 80 percent lower than the moduli before HVS testing. The reduction in moduli reflects the fatigue damage produced by the HVS trafficking.

Backcalculated AC moduli from FWD deflections taken several weeks after HVS trafficking indicate a slight recovery. Modulus values increased from about 1000 MPa immediately after the completion of HVS trafficking to about 1500 MPa three months later.

Moduli of the aggregate base layers are shown in Figure 37. During Stage 2, moduli ranged from 300 to 400 MPa for the three load levels. Higher moduli were obtained for the lighter load during the dry period and during the first weeks of water infiltration (July-August 1999). Thereafter, all three load levels yielded similar aggregate base moduli. Aggregate base moduli after HVS trafficking dropped to values between 60 and 100 MPa. This reduction is likely due to an increase in moisture content from infiltrated water, and by a change in stress state resulting from asphalt concrete damage. Moduli of the aggregate base recover somewhat, likely due to reduction in moisture content since water infiltration was stopped after HVS trafficking, as noted earlier.

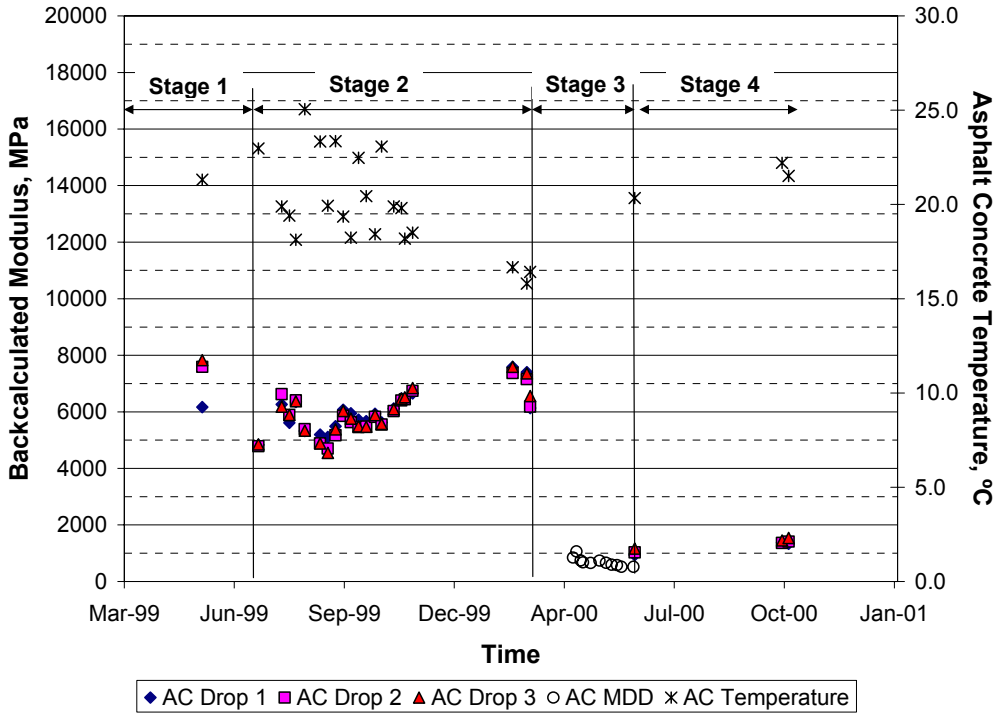


**Figure 36. AC moduli backcalculated from FWD deflections.**

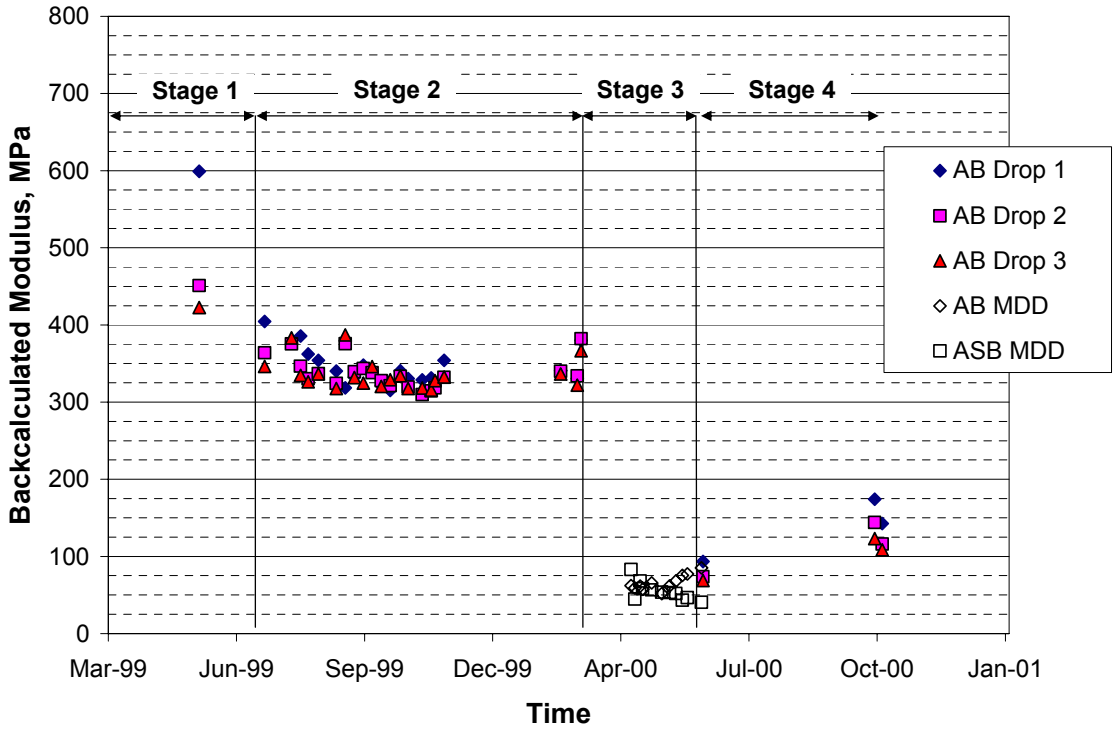


**Figure 37. Moduli of aggregate base.**

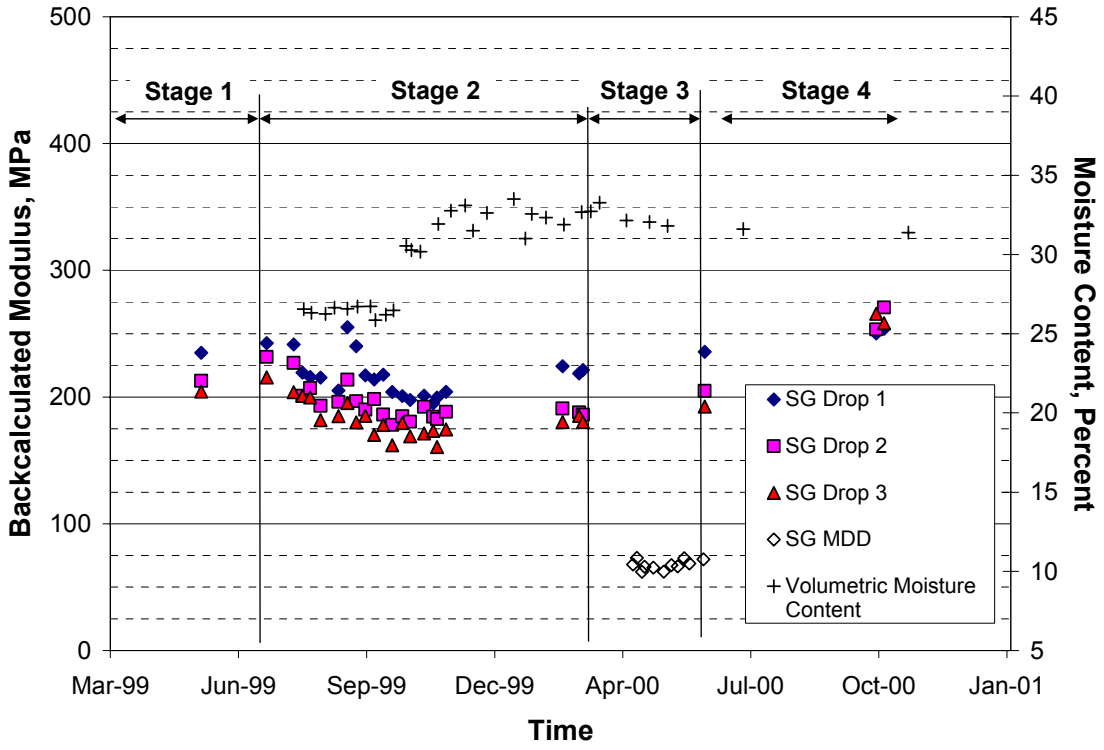


**Figure 38. Moduli of subgrade.**

Figure 38 shows the moduli and volumetric moisture contents of the subgrade layer for the various stages of testing. Subgrade moduli ranged from 150 to 250 MPa for Stages 1, 2, and 4. Moduli decrease slightly during Stage 2. This decrease is related to an increase in moisture content, as seen in the figures. A 20 percent reduction in modulus was obtained for a volumetric moisture content increase of 7 percent (from 26 percent to 33 percent).

Backcalculated moduli from MDD in-depth deflections (Stage 3) are also presented in the figures for comparison with the FWD results at the end of HVS testing (Stage 4). Backcalculated moduli using both methods were similar for the asphalt concrete and aggregate base layers. Moduli of the asphalt concrete backcalculated from MDD deflections were lower than those backcalculated from FWD deflections. The results were expected since the time of loading associated with the HVS loading is considerably larger than that used for the FWD testing.

Backcalculated moduli for the subgrade were lower based on the MDD deflections as compared to those calculated from FWD deflections. The differences may be attributed in part to the procedures used to estimate subgrade moduli using the MDD deflection data. In this instance, since the MDD at the subgrade level was inoperable, it was necessary to calculate subgrade moduli based on deflection data obtained for the upper layers. The subgrade moduli for Section 544 are, however, similar to those obtained for Section 543 where the subgrade moduli were estimated from MDD data at the subgrade level. Accordingly, differences may be due to other factors such as stress state differences and rate of loading effects.

### 3.6 Forensic Activities

Forensic activities included core extraction, dynamic cone penetrometer testing, moisture content measurements, and trenching of the test section for direct observation of deformations in the pavement structure. Figure 39 shows a layout of the forensic activities.

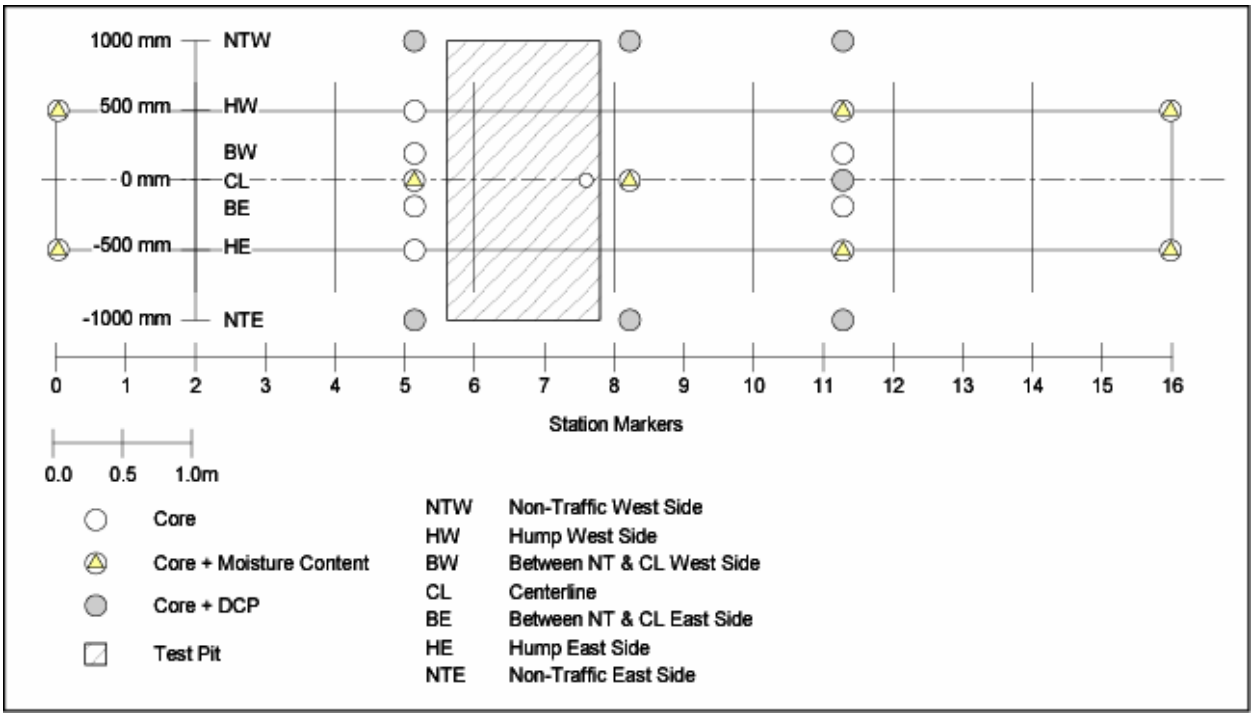


**Figure 39. Layout of forensic activities for Section 544.**

### 3.6.1 Air-Void Contents from Extracted Cores

Figure 40 summarizes air-void content data for all bound layers. Lower air-void contents for cores from the ARHM-GG mix were observed within the trafficked area as compared to cores from outside the trafficked area; Figure 39 shows locations at which the cores were obtained. A significant reduction in air-void content (from 11 to 15 percent at the start of HVS trafficking to about 7 to 9 percent at the end of HVS trafficking) was observed along the centerline. The high initial air-void contents observed in the ARHM-GG were anticipated and reported earlier in Reference (*9*). For the top and bottom lifts, of the dense graded asphalt concrete, very small differences were observed in the cores from the trafficked and non-trafficked areas.

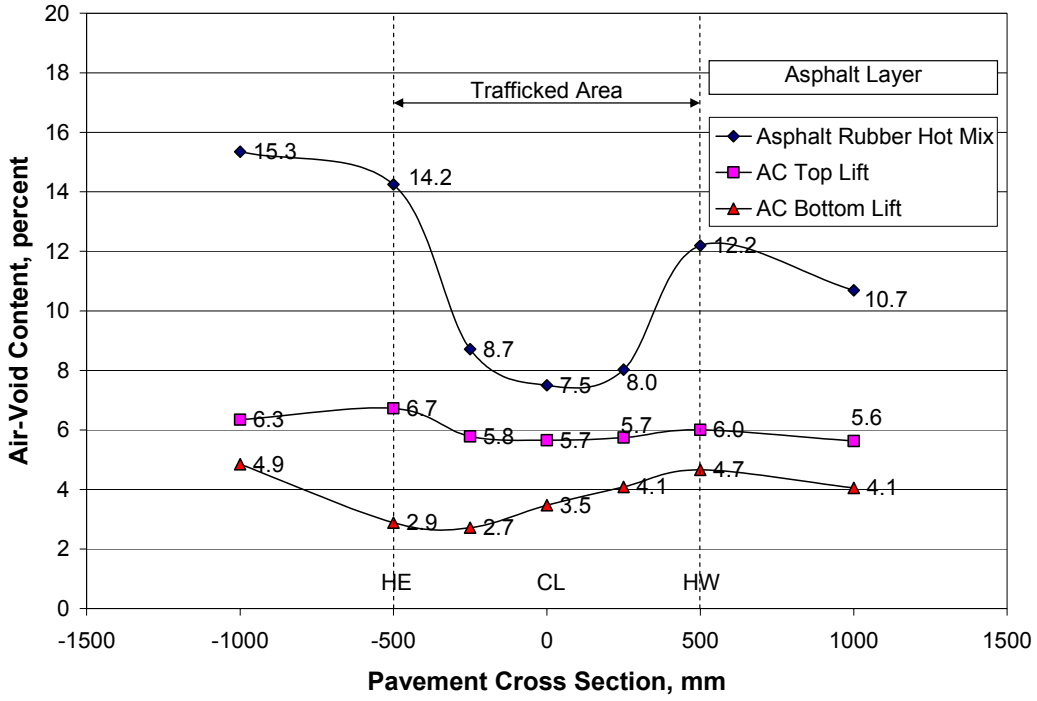


**Figure 40. Average air-void contents across Section 544 after HVS trafficking.**

### 3.6.2 Bonding between Asphalt Layers

All the cores extracted along the centerline of the trafficked area exhibited no bond between the asphalt layers. However, for the cores obtained at a distance ±200 mm from the centerline, bonding between the ARHM-GG top layer and the top DGAC lift was observed.

As in earlier studies,(*9*) no bond was present between the top and bottom lifts of DGAC. For the cores obtained along the boundary between the trafficked and non-trafficked areas and outside the trafficked area, the cores were intact throughout the asphalt layers. As noted in earlier studies, this bond was relatively weak and was easily ruptured under HVS loading. In cores obtained from cracked areas, cracking was present throughout the depth of the cores.

### 3.6.3 Dynamic Cone Penetrometer (DCP) Data

Figures 41–43 present Dynamic Cone Penetrometer (DCP) data for Section 544 (refer to Figure 39 for DCP test locations). The DCP plan permitted comparison of the penetration rates of the unbound layers in the non-trafficked and trafficked areas.

Table 10 contains a summary of DCP penetration rates for the aggregate base, aggregate subbase, and subgrade after HVS trafficking. The data indicate lower penetration rates for the aggregate subbase, followed by the aggregate base, and the subgrade. Lower penetration rates indicate higher resistance to shear. In this instance, the aggregate subbase likely has a higher resistance to shear than the aggregate base because of the high moisture content due to water infiltration of the base. For the aggregate base, consistently lower penetration rates were obtained along the trafficked area centerline than in the non-trafficked areas. This difference in penetration rates in the aggregate base is likely due to an increase in compaction produced by HVS trafficking.

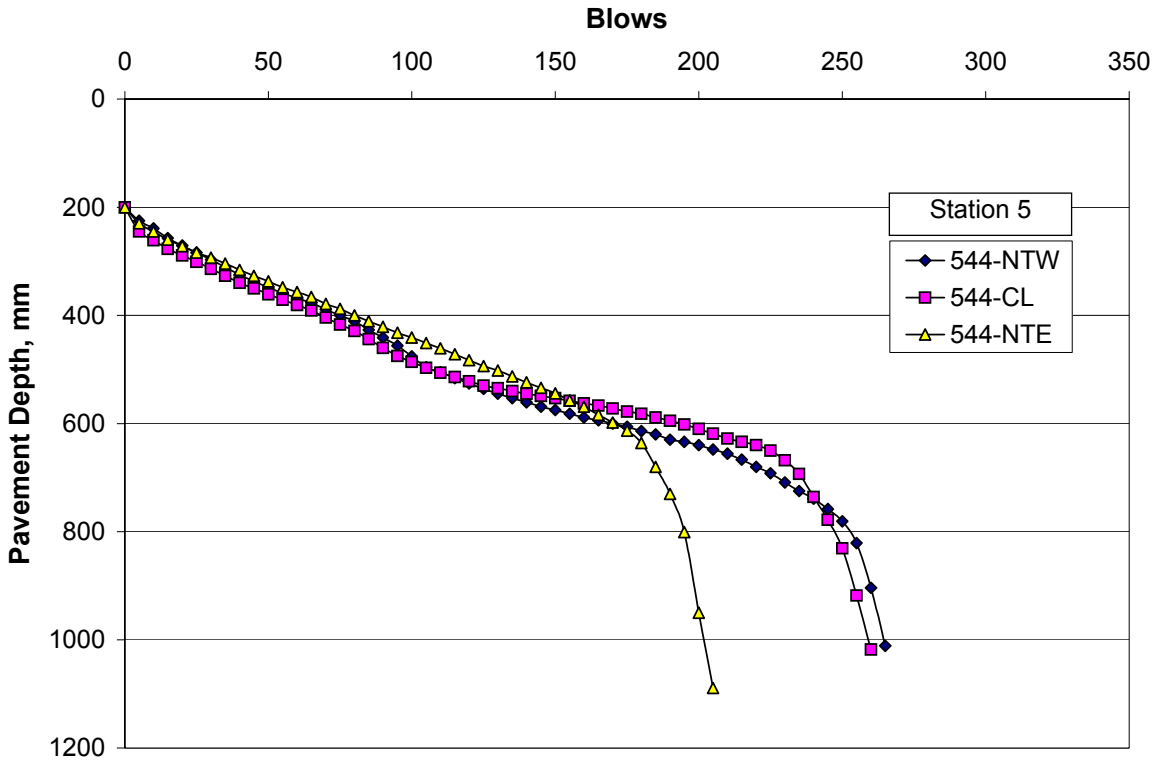


**Figure 41. DCP results for Section 544, Station 5.**

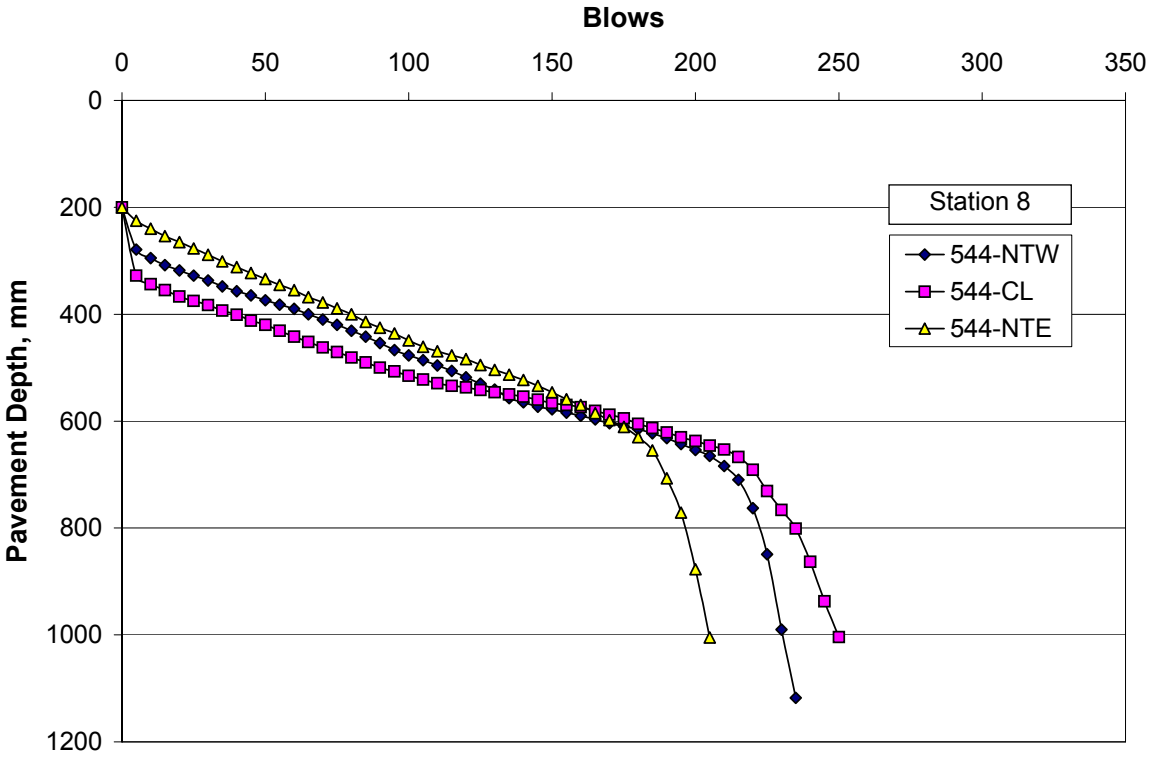


**Figure 42. DCP results for Section 544, Station 8.**

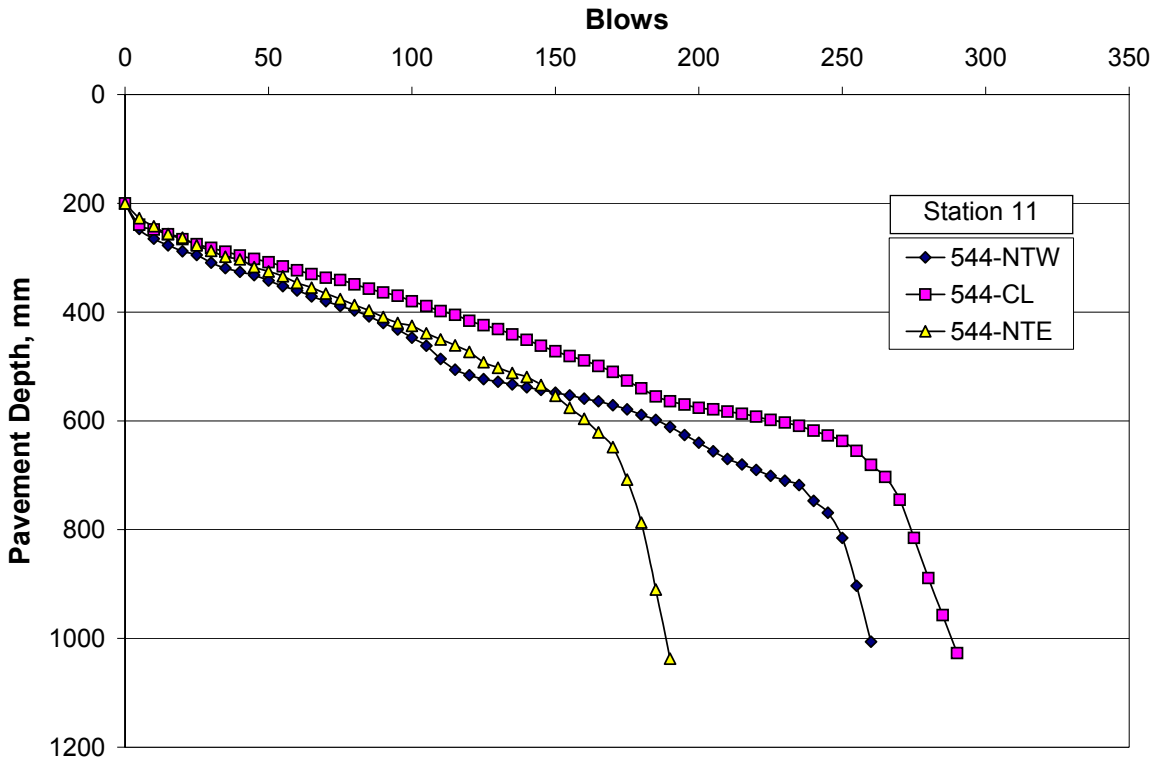


**Figure 43. DCP results for Section 544, Station 11.**

**Table 10 Summary of DCP Penetration Rates**

| DCP Test Location* | | Penetration Rate (mm/blow) | | |
|---|---|---|---|---|
| | | Aggregate Base | Aggregate Subbase | Subgrade |
| **Station 5** | NTW | 2.5 | 1.3 | 15.5 |
| | CL | 2.4 | 1.0 | 16.1 |
| | NTE | 2.2 | 2.4 | 20.8 |
| **Station 8** | NTW | 2.0 | 1.3 | 20.9 |
| | CL | 1.9 | 1.4 | 10.3 |
| | NTE | 2.3 | 1.0 | 17.4 |
| **Station 11** | NTW | 2.0 | 1.8 | 16.0 |
| | CL | 1.6 | 1.0 | 13.3 |
| | NTE | 2.1 | 2.4 | 22.2 |
| **Summary** | NTW | 2.2 | 1.5 | 17.4 |
| | CL | 2.0 | 1.1 | 13.3 |
| | NTE | 2.2 | 1.9 | 20.1 |
| | Average across all tests | 2.1 | 1.5 | 16.9 |

*Refer to Figure 25 for explanation of test locations.

Table 11 summarizes DCP penetration rates for DCP tests conducted 10 days after construction of the sections and during the forensic activities for the Goal 3 HVS program. It must be reiterated that these tests were conducted when no water infiltration from the surface was allowed.

**Table 11 DCP Penetration Rates Obtained under Dry Conditions**

| **Layer** | **Penetration Rate (mm/blow)** | |
|---|---|---|
| | **10 Days After Construction** | **During Forensic Activities for Goal 3 Program** |
| Aggregate Base | 2.3 | 2.2 |
| Aggregate Subbase | 3.4 | 1.3 |
| Subgrade | 17.7 | 18.2 |

Comparison of DCP results from Section 544 with those from previous test sections indicates a difference in the resistance of the aggregate subbase layer. This probably results from densification of this layer during earlier trafficking. These results also show that DCP penetration rates do not differentiate between dry and wet conditions of the aggregate base. DCP tests were conducted one week after water infiltration was ceased. It is possible that moisture content was reduced during that time which would increase the strength of the material. However, results of FWD testing indicated lower moduli for the aggregate base several weeks after ceasing water infiltration. Thus, case must be taken in interpreting DCP penetration rates to establish DCP-modulus relationships.

### 3.6.4 Trench Data

After the completion of HVS trafficking, a transverse test pit was dug in order to enable direct observation of the pavement layers, as shown in Figure 39. Measurements from the trench were used to estimate thickness and rutting in the pavement layers. Figures 44 and 45 show

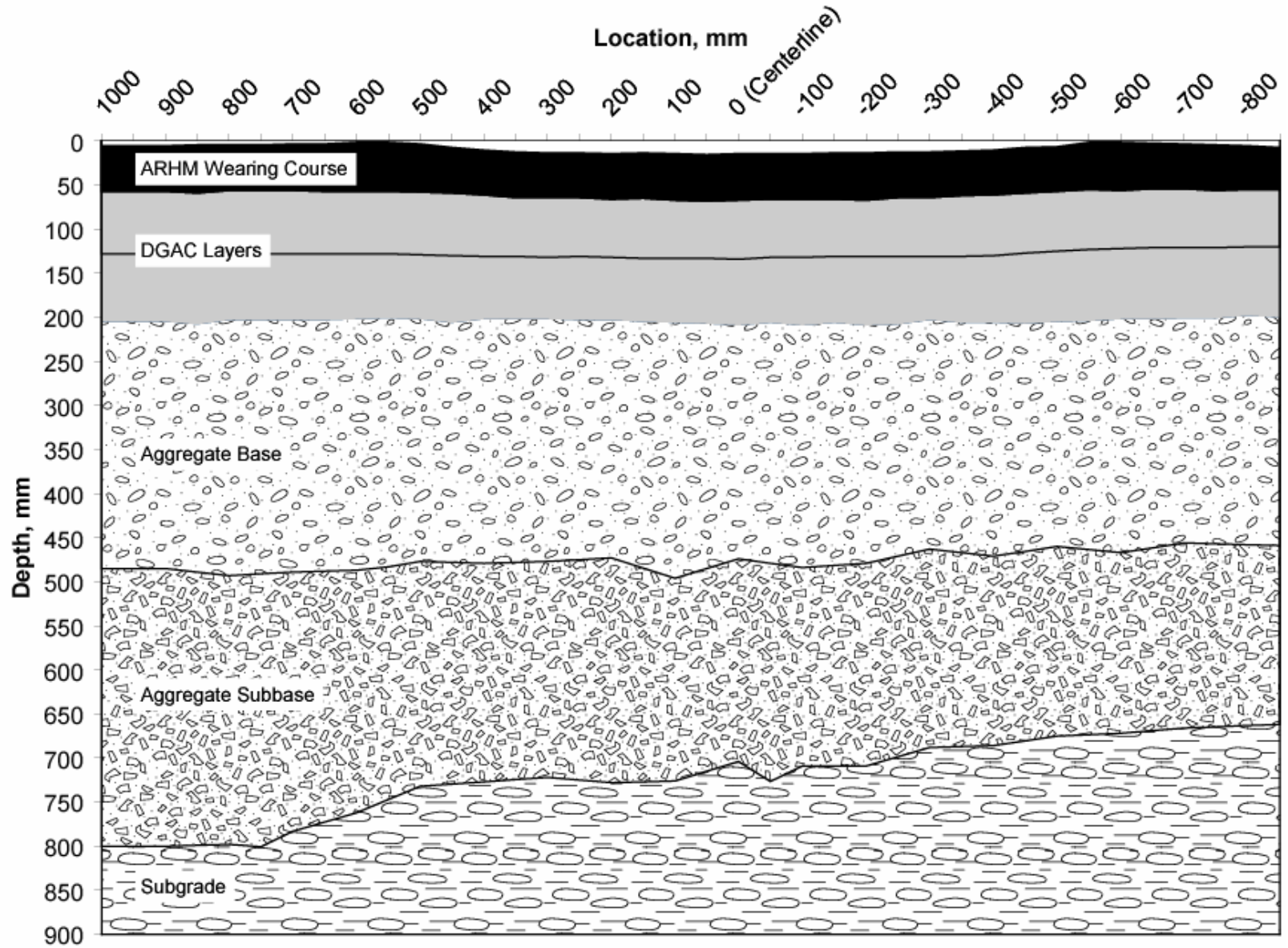


**Figure 44. Trench data, south face of trench at Station 5, Section 544.**

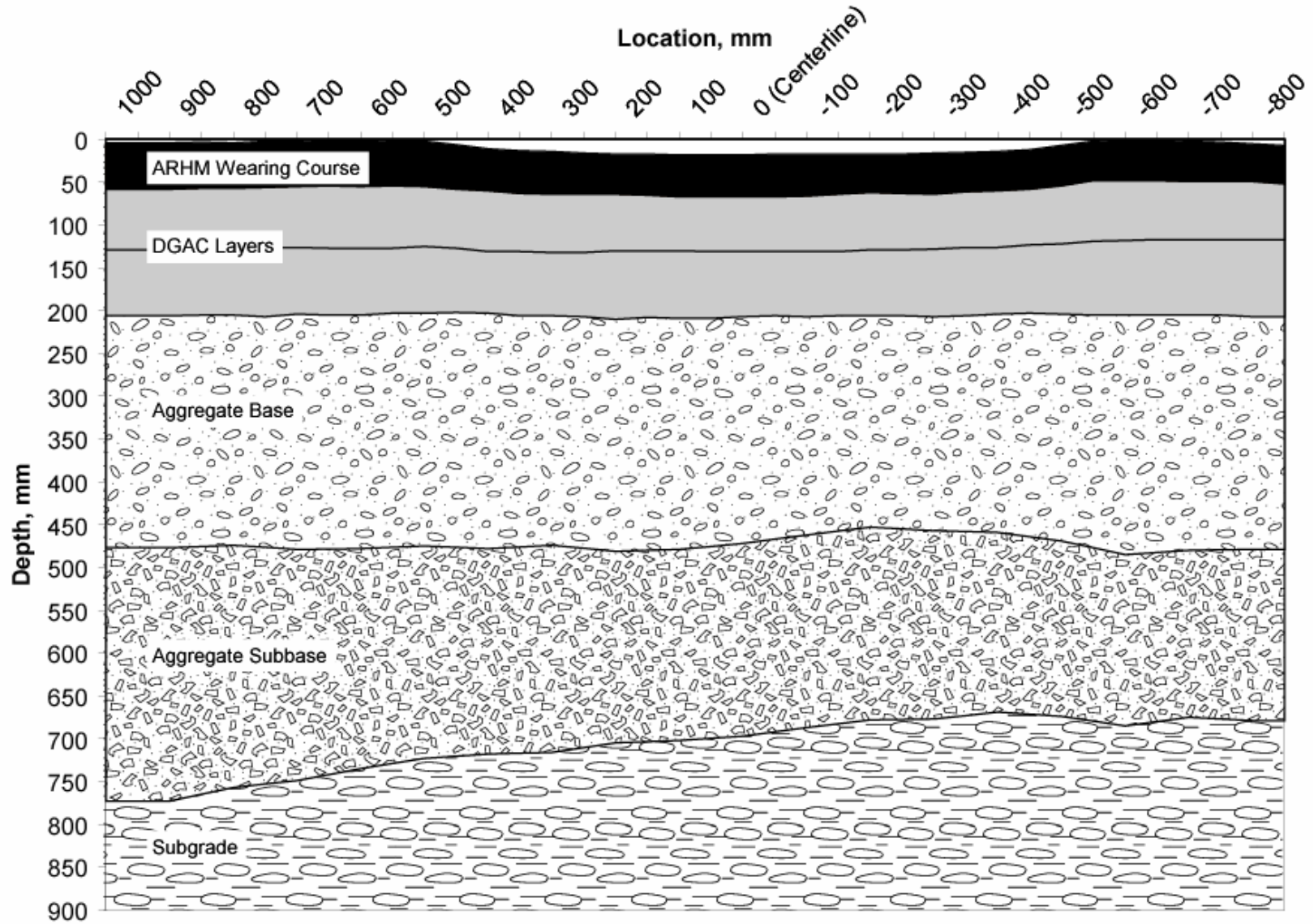


**Figure 45. Trench data, north face of trench at Station 8, Section 544.**

profile data at the interface of each layer at the completion of HVS trafficking. During the data collection process, it was difficult to establish the boundary between the asphalt concrete and the aggregate base due to roughness at the interface of the two layers. The profiles show that the subbase thickness varied considerably across the section. Differences in subbase thickness were anticipated and reported in previous Reports (*10–13*).

Figure 46 summarizes average layer thicknesses and standard deviations for seven distinct locations across the pavement section (shown in Figure 39). Measurements taken outside the trafficked areas (NTW and NTE) indicate variability of thickness across the section during construction. With this variability occurring without trafficking, it is difficult to establish the level of rutting of the individual layers. In addition, measurement variability and roughness at the layer interfaces make it difficult to establish the level of rutting in the individual layers, particularly in the unbound layers.

Based on the information provided by the MDDs and air-void content data, some rutting may have occurred in the ARHM-GG layer due to initial high air-void contents present in this layer before trafficking and the lower air-void contents measured after trafficking. However, based on the variability in the thickness data, this could not be verified. Thickness data for the top and bottom lifts of asphalt concrete indicate that these layer developed some rutting. MDD data indicate that 6 mm occurred in the asphalt concrete layers.

MDD data showed that about 5 mm of permanent deformation occurred at the top of the aggregate base. This could not be verified with the thickness data because standard deviations for the thickness measurements of the aggregate base ranged from 1 to 11 mm, with most of the variability occurring along the centerline of the section.

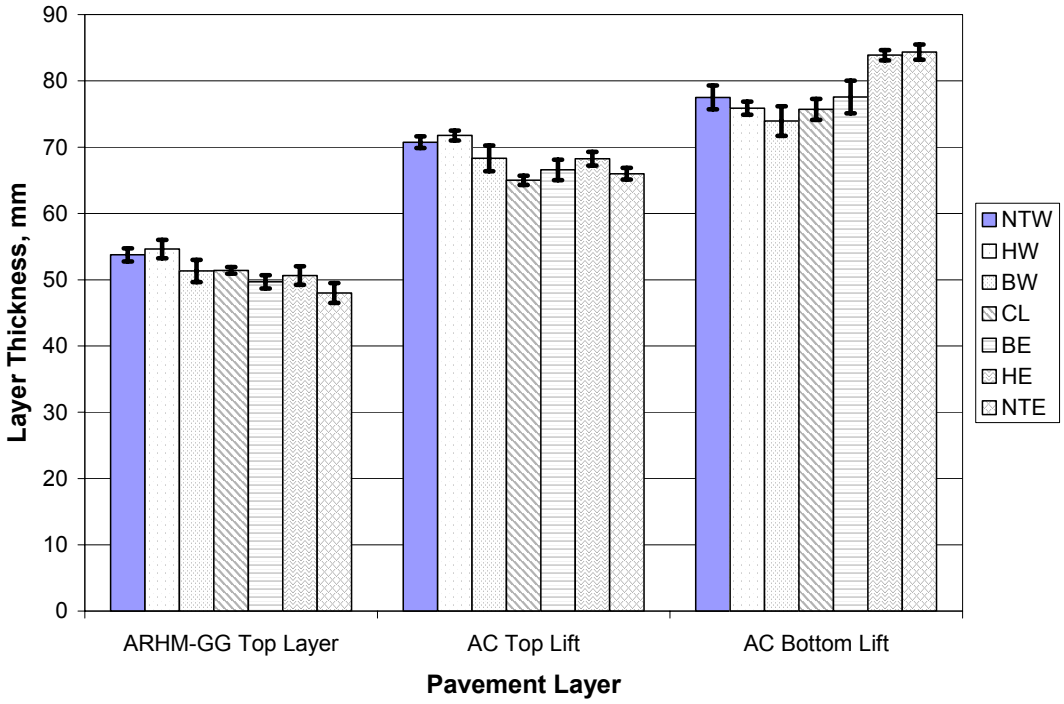


**Figure 46a. Asphalt layers.**

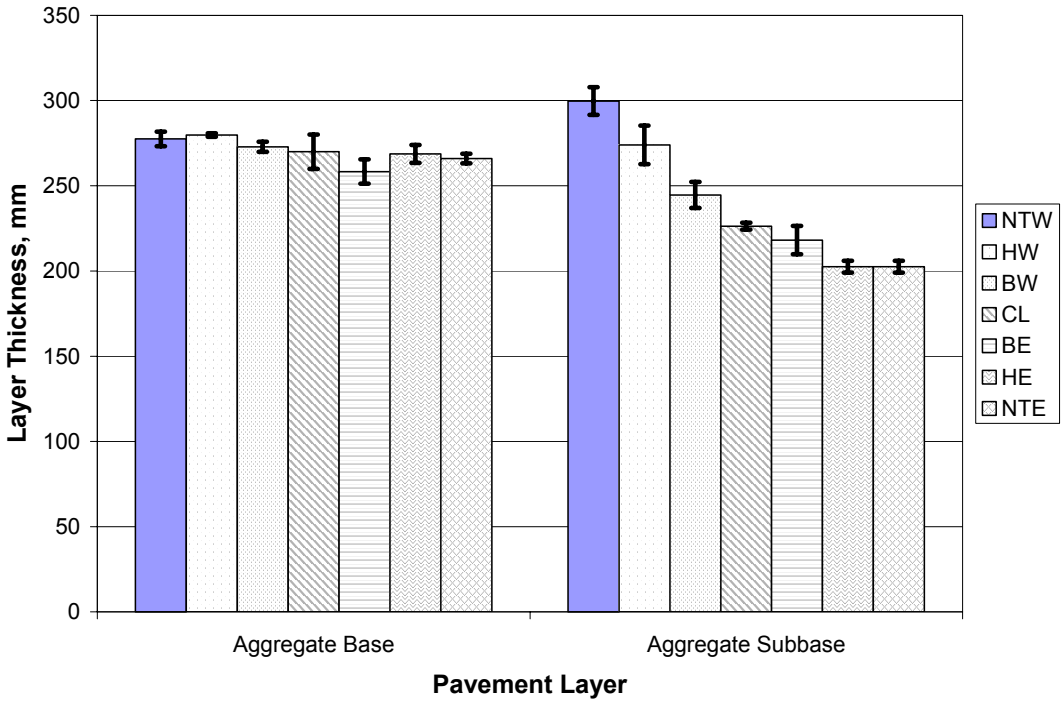


**Figure 46b. Untreated aggregate layers.**

**Figure 46. Measured layer thicknesses in the test pit.**

## 4.0 PERFORMANCE EVALUATION AND MECHANISTIC ANALYSIS

At the end of HVS testing, Section 544 had been subjected to 176,000 applications of the 40-kN load, 211,000 applications of the 80-kN load, and 718,000 repetitions of the 100-kN load. This corresponded to 37.7 million ESALs using the Caltrans 4.2 load equivalency factor. The number of ESALs to failure, based on Caltrans criteria, was 20.3 million for surface rutting (12.5 mm) and 14.3 million for cracking (2.5 $m/m^2$). Thus, Section 544 was considered to have failed by fatigue cracking rather than by surface rutting.

Comparison of the performance of Section 544 with that of Section 543 (*6*) indicated that the modes of failure were different. For Section 543, the numbers of ESALs to failure were 18.7 and 35.8 million for surface rutting and fatigue cracking, respectively, whereas as noted above, ESALs to failure for Section 544 were 20.3 and 14.3 for rutting and cracking, respectively.

Section 543 failed first by surface rutting due to the poor performance (stripping and fine particle contamination) of the ATPB layer under wet conditions and trafficking. However, the performance data also showed that the ATPB layer initially provided this section with improved fatigue resistance which was lost once the stiffness of the ATPB layer was reduced by stripping and fines intrusion.

In Reference (*6*), an analysis was conducted in which the 75-mm ATPB layer was replaced by 40 mm of DGAC. The next section includes a mechanistic-based analysis to compare the response and performance of this alternative section with that of Section 544.

### 4.1 Mechanistic-Based Analysis

For the analyses, the two pavement systems were assumed to be multi-layer elastic structures. Selected pavement responses for performance assessment were the tensile strain at the bottom of the asphalt concrete layer, and vertical compressive stress on top of the unbound

layers. The pavement considered are: 1) the pavement structure used for Section 544; and 2) the pavement structure with increased AC thickness considered for an alternative to Section 543. Table 12 summarizes the pavement thickness and layer moduli for the two cases. Layer moduli are based on average backcalculated moduli determined from FWD testing.

**Table 12 Summary of Pavement Structures for Analysis.**

| Layer | Thickness, mm | Moduli Before HVS Testing, MPa | Moduli After HVS Testing, MPa |
|---|---|---|---|
| ***Structure 544*** | | | |
| AC | 200 | 5900 | 1030 |
| AB | 532 | 338 | 74 |
| SG | | 195 | 205 |
| ***Modified Structure 543*** | | | |
| AC | 240 | 5900 | |
| AB | 368 | 300 | |
| SG | | 170 | |

Table 13 summarizes pavement responses under a 40-kN load for the three cases considered (Section 544 dry and wet and one scenario for the modified Section 543). Pavement responses indicate that the pavement with the increased thickness of asphalt concrete would perform better than the section with thicknesses representative of those of Section 544. Lower tensile strains in asphalt and lower stresses on top of the aggregate base indicate longer fatigue performance of the asphalt concrete layer and longer rutting performance of the aggregate base layer.

**Table 13 Summary of Pavement Responses under 40-kN Load**

| Pavement Response | Case I | | Case II | |
|---|---|---|---|---|
| | Before | After | Before | After |
| Tensile Strain at Bottom of AC, μstrain | 67 | 352 | 50 | - |
| Vertical Stress at Top of AB, kPa | 65 | 75 | 43 | - |
| Vertical Stress at Top of SG, kPa | 27 | 68 | 28 | - |

### 4.1.1 Fatigue Analysis

The fatigue analysis and design system used in this report is presented in Reference (*10*) and is summarized in Figure 47.

For this particular analysis, a design reliability of 50 percent has been assumed; this results in reliability multiplier of 1.0. The laboratory fatigue life equation for the mixes used in the simulation is:

$$\ln N = -21.9295 - 0.109996\,AV - 4.14248 \ln \varepsilon$$

where $N$ is the number of repetitions to failure obtained from laboratory fatigue beam tests tested under strain control, $AV$ is the percent air-void content in the mix, and $\varepsilon$ is the tensile strain at the

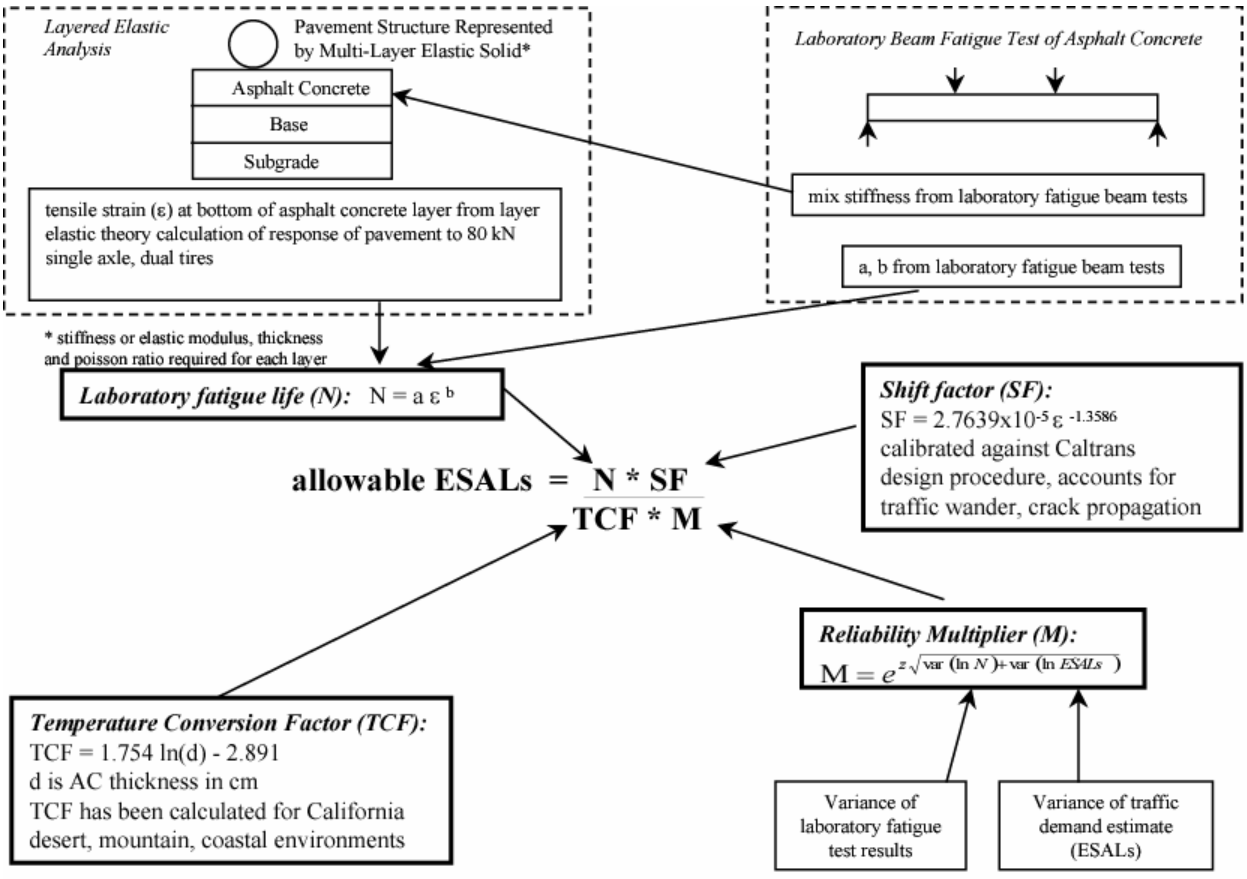


**Figure 47. Methodology followed in the fatigue analysis system to determine ESALs.**

bottom of the asphalt concrete. The shift factor (*SF*) is obtained from the following expression (*14*):

$$SF = 3.1833 \times 10^{-5} \varepsilon^{-1.3759}$$

and the temperature conversion factor (TCF) equation which has been utilized is (*14*):

$$TCF = 1.754 \ln(d) - 2.891$$

where $d$ = AC layer thickness, cm. Results of the simulation process are summarized in Table 14.

**Table 14 Summary of Calculation of ESALs using UCB Fatigue Analysis System**

| Case | μstrain | Air-Void Content, % | ln N | N, millions | Shift Factor | AC Thickness, cm | Temperature Conversion Factor | M | ESALs, millions |
|---|---|---|---|---|---|---|---|---|---|
| I | 67 | 4.6 | 17.40 | 35.9 | 17.6 | 20.0 | 2.36 | 1 | 267 |
| II | 50 | 4.6 | 18.61 | 120.7 | 26.3 | 24.0 | 2.68 | 1 | 1,185 |

These results indicate that the section with the increased thickness of asphalt concrete (asphalt concrete in lieu of the ATPB layer) would perform better in fatigue than Section 544, with about a factor of 4 increase in ESALs. As discussed in Reference (*6*), the section in which the ATPB has been replaced with an equivalent thickness of AC eliminates the potential of reduced stiffness in the ATPB due to poor drainage. This increased thickness provides the same benefits provided by the ATPB: longer fatigue life in the asphalt concrete layer and additional cover that results in a reduction of the vertical stresses on top of the unbound layer.

## 4.2 Rutting Analysis

An assessment of the rutting on top of the aggregate base has been made using vertical stress computer at this location. While performance equations for estimating rutting in the

unbound layers are still under development, a simplified analysis has been included for Section 544.

For a 40-kN load (one-half of an 80-kN standard axle load), the computer vertical compressive stresses on top of the aggregate base were 65 kPa before HVS testing and 75 kPa after HVS testing (see Table 13). In Section 544, the majority of the rutting occurred under HVS loading of 100 kN. For this condition, the vertical stress on top of the aggregate base was likely of the order of 150 kPa. This estimated vertical stress produced a level of rutting of 6 mm on top of the aggregate base for the section with the increased AC thickness (Case II, Table 13) resulting in an estimated stress of 43 kPa under a 40-kN load and 101 kPa under the 100-kN load. Therefore, the new section would be estimated to exhibit less rutting on top of the aggregate base than Section 544.

## 5.0 CONCLUSIONS AND RECOMMENDATIONS

This report summarizes the results of accelerated pavement testing and associated analyses for Section 544 of the Goal 5 research project. This flexible pavement structure did not include the 75-mm ATPB layer between the asphalt concrete and the aggregate base layer, which has been required in Caltrans designs for new pavement structures. The report includes the analysis for the four stages of testing considered in the Goal 5 Test Plan for Section 544. Results of the accelerated pavement testing form the basis for recommendations regarding the use of ATPB layers.

Testing for Section 544 began in March 2000 and was completed in June 2000. Under HVS loading, a total of $1.1 \times 10^6$ repetitions were applied to the section: 176,000 repetitions of a 40-kN load; 211,000 repetitions of an 80-kN load, and 718,000 repetitions of a 100-kN load. The section was trafficked under a "wet base" condition accomplished using a water infiltration system. The wet conditions were intended to simulate precipitation for an average peak week of 51.3 mm, which is typical in Eureka, California.

Comparisons of the permanent deformation data for an undrained section under dry and wet base conditions provides the basis for assessing the detrimental effects of increased moisture content on the rutting performance of the pavement section. For these conditions, pavement life was reduced from about 95 million ESALs to 20 million ESALs. This results in part from an increase in elastic deflections under wet base condition as compared to a similar test section with dry base conditions.

Permanent deformation data for the undrained (Section 544) and drained (Section 543) sections illustrated a difference in performance among the two sections. For Section 544, the permanent deformation rate decreased with the number of load applications. Section 543 exhibited a permanent deformation rate which increased at a faster rate than Section 544 once

trafficking with the 100-kN load was applied. Prior to the 100-kN loading, the drained section (543) performed better than the undrained section (544). However, once the stiffness of the ATPB was reduced by stripping and intrusion of fines, the permanent deformation rate rapidly increased in the section. Elastic deflections measured at the beginning of HVS testing indicated that the undrained section (544) had higher elastic deflections than the drained section (543). Measured elastic deflections however, were similar for both sections at the end of HVS testing. This similarity in response indicates that as the stiffness of the ATPB was reduced under 100-kN loading, for the reasons stated above, it behaved similar to an aggregate base. Analysis of the results from the backcalculation process resulted in a similar conclusion.

## 5.1 Conclusions

From the results of the test on Section 544 and associated response and performance analyses, the following conclusions are drawn:

1. The undrained section (544) failed first in fatigue cracking, rather than by surface rutting as did Section 543. Fatigue cracking resulted from the increase in elastic deflections because of increased moisture content in the aggregate base.
2. Permanent deformation rates were lower for the undrained section than for the drained section under the 100-kN trafficking load. Stiffness of the ATPB in the drained section was reduced significantly due to stripping and to fines intrusion, which produced an increase in the permanent deformation rate in the drained section. Before the ATPB stripped in Section 543, the performance of this section was superior to that of the undrained section.
3. An increase in the asphalt concrete thickness in the undrained section would provide this type of section better performance under fatigue cracking and aggregate base

rutting. Mechanistic-empirical analyses indicated that the increased thickness reduces both the tensile strain at the bottom of the asphalt concrete layer and the vertical stresses on top of the aggregate base which in turn increases the performance of the pavement section for both fatigue cracking and surface rutting.

4. Ground penetrating radar (GPR) testing was able to predict the range of moisture contents present in the aggregate base and subbase layers. Average absolute errors were less than 1 percent. The inaccuracy of the GPR derived estimates may be caused by varying thickness in the aggregate base and subbase or by uneven boundaries between the layers. Regardless of the inaccuracy, the GPR technique can be an effective non-destructive method for estimating moisture contents in the untreated base materials. Errors of ± 2 percent in moisture content of untreated aggregate base materials are accurate enough for engineering applications. Other methods for estimating moisture contents in the aggregate bases such as the hydroprobes were not effective in measuring moisture content in these layers.
5. Falling weight deflectometer (FWD) testing was effective in establishing the structural condition of the pavement sections during all stages of testing. Changes in the moduli of the layers due to moisture content changes and trafficking were effectively determined by the device.

## 5.2 Recommendations

1. Undrained sections can provide excellent pavement performance without using drainage layers between the asphalt concrete and the aggregate base provided the section is properly designed. To mitigate infiltration of surface water into the untreated base, the permeability of the asphalt concrete can be reduced by means of

improved compaction. Also, sufficient thickness of asphalt concrete can mitigate the potential for load associated cracking. In addition, improved compaction in the aggregate base can reduce the potential for rutting in the untreated aggregate and will also contribute to improved fatigue resistance.

2. GPR has a potential for measuring moisture content in the aggregate base and subbase layers. However, techniques for easily and rapidly interpreting GPR data are needed.
3. Continue using FWD testing for the structural evaluation of pavements.

## 6.0 REFERENCES


1. Harvey, J., M.O. Bejarano, A. Ali, "Test Plan for Goal 5: Performance of Drained and Undrained Flexible Pavement Structures under Wet Conditions", Pavement Research Center, Cal/APT Program, Institute of Transportation Studies, University of California, Berkeley.

2. Harvey, J., Chong, A., Roesler, J. *Climate Regions for Mechanistic-Empirical Pavement Design in California and Expected Effects on Performance.* Draft report prepared for California Department of Transportation. Pavement Research Center, CAL/APT Program, Institute of Transportation Studies, University of California, Berkeley. June 2000.

3. Harvey, J. T., L. du Plessis, F. Long, S. Shatnawi, C. Scheffy, B-W. Tsai, I. Guada, D. Hung, N. Coetzee, M. Reimer, and C. L. Monismith. *Initial CAL/APT Program: Site Information, Test Pavement Construction, Pavement Materials Characterizations, Initial CAL/APT Test Results, and Performance Estimates.* Report prepared for the California Department of Transportation. Report No. RTA-65W485-3. Pavement Research Center, CAL/APT Program, Institute of Transportation Studies, University of California, Berkeley, June 1996, 305 pp.

4. Harvey, J., M. O. Bejarano, A. Fantoni, A. Heath, and H. C. Shin. *Performance of Caltrans Asphalt Concrete and Asphalt-Rubber Hot Mix Overlays at Moderate Temperatures – Accelerated Pavement Testing Evaluation.* Draft report submitted to California Department of Transportation. Pavement Research Center, CAL/APT Program, Institute of Transportation Studies, University of California, Berkeley. July 2000.

5. Harvey, John T., Louw du Plessis, Fenella Long, John A. Deacon, Irwin Guada, David Hung, Clark Scheffy. *CAL/APT Program: Test Results from Accelerated Pavement Test on Pavement Structure Containing Asphalt Treated Permeable Base (ATPB) Section 500RF.* Report No. RTA-65W485-3. Report Prepared for California Department of Transportation. Pavement Research Center, CAL/APT Program, Institute of Transportation Studies, University of California, Berkeley. June 1997.

6. Harvey, J., J. Prozzi, J. Deacon, D. Hung, I. Guada, L. du Plessis, F. Long, and C. Scheffy. *CAL/APT Program: Test Results from Accelerated Pavement Test on Pavement Structure Containing Aggregate Base (AB)--Section 501RF.* Report prepared for the California Department of Transportation. Pavement Research Center, CAL/APT Program, Institute of Transportation Studies, University of California, Berkeley. Draft submitted September 1997. Final submitted April 1999.

7. Harvey, J., I. Guada, C. Scheffy, L. Louw, J Prozzi, and D. Hung. *CAL/APT Program: Test Results from Accelerated Pavement Test on Pavement Structure Containing Asphalt Treated Permeable Base--Section 502CT.* Draft report submitted to California Department of Transportation. Pavement Research Center, CAL/APT Program, Institute of Transportation Studies, University of California, Berkeley. February 1998.

8. Harvey, J., D. Hung, J. Prozzi, L. Louw, C. Scheffy, and I. Guada. *CAL/APT Program: Test Results from Accelerated Pavement Test on Pavement Structure Containing Untreated Aggregate Base--Section 503RF.* Draft report submitted to California Department of Transportation. Pavement Research Center, CAL/APT Program, Institute of Transportation Studies, University of California, Berkeley. December 1997.

9. Rubin, Y., S. Hubbard, M. Riemer, J. Harvey, and K. Grote. *Calibration of Surface Ground Penetrating Radar for Measuring Water Content Using Buried Reflectors.* Draft report submitted to California Department of Transportation. Pavement Research Center, CAL/APT Program, Institute of Transportation Studies, University of California, Berkeley. April 1999.

10. Manuel O. Bejarano, John T. Harvey, Abdikarim Ali, Mark Russo, David Mahama, Dave Hung, and Pitipat Preedonant. *Performance of Drained and Undrained Flexible Pavement Structures under Wet Conditions Test Data from Accelerated Pavement Test Section 543-Drained*. Draft report prepared for the California Department of Transportation. Pavement Research Center, Institute of Transportation Studies, University of California Berkeley, University of California Davis. February 2004.

11. Manuel O. Bejarano, John T. Harvey, Abdikarim Ali, Mark Russo, David Mahama, Dave Hung, and Pitipat Preedonant. *Performance of Drained and Undrained Flexible Pavement Structures under Wet Conditions Test Data from Accelerated Pavement Test Section 545-Undrained*. Draft report prepared for the California Department of Transportation. Pavement Research Center, Institute of Transportation Studies, University of California Berkeley, University of California Davis. June 2004.

12. Inge, E. H., and Y. R. Kim. "Prediction of Effective Asphalt Layer Temperature." *Transportation Research Record No. 1473.* Transportation Research Board, National Research Council, Washington D.C. 1995.

13. Ullidtz, P. *Pavement Analysis.* Elsevier Publishing Company, 1987.

14. Harvey, J. T., Deacon, J. A., Tsai, B-W., Monismith, C. L. *Fatigue Performance of Asphalt Concrete Mixes and Its Relationship to Asphalt Concrete Pavement Performance in California*. Report prepared for the California Department of Transportation. Report No. RTA-65W485-2. Pavement Research Center, CAL/APT Program, Institute of Transportation Studies, University of California Berkeley, January 1996, 189 pp.